A Quantitative Design and Analysis of Magnetic Nanoparticle Heating Systems

by

Shahriar Rohinton Khushrushahi

Submitted to the Department of Electrical Engineering and Computer Science
in partial fulfillment of the requirements for the degree of

Masters of Science in Electrical Engineering

at the

MASSACHUSETTS INSTITUTE OF TECHNOLOGY

October 2005
[February 2006]

Author .....
Department of Electrical Engineering and Computer Science
Oct 6, 2005

Certified by .....
Kimberly Hamad-Schifferli
Assistant Professor of Mechanical Engineering
Thesis Supervisor

Accepted by .....
Arthur C. Smith
Chairman, Department Committee on Graduate Students

A Quantitative Design and Analysis of Magnetic Nanoparticle Heating Systems

by

Shahriar Rohinton Khushrushahi

Submitted to the Department of Electrical Engineering and Computer Science
on Oct 6, 2005, in partial fulfillment of the
requirements for the degree of
Masters of Science in Electrical Engineering

Abstract

Magnetic particles under the influence of an alternating magnetic field act as localized heating sources due to various loss mechanisms. This effect has been extensively investigated in hyperthermia studies over the past decades and has recently been applied at the molecular level to control the dehybridization of DNA molecules. As a result, it has the potential of controlling and studying biological systems.

To ensure that the nanoparticles are the only source of heat requires a very efficient system that minimizes heat transfer from sources other than the magnetic field. A quantitative analysis of the requirements and the design of such a system was investigated and tested experimentally. Although the results were affected by transmission line effects, the theory supporting the approach is sound and explains the crucial parameters that are necessary for optimizing localized ferromagnetic nanoparticle heating.

Thesis Supervisor: Kimberly Hamad-Schifferli
Title: Assistant Professor of Mechanical Engineering

Acknowledgments

For the past two years I have been in the direct path of the renowned MIT firehose, and there are a bunch of people who have not only made it bearable but enjoyable.

I want to first thank Kim for allowing me to join her group. Despite my background being limited to Electrical Engineering, I was keen on getting into a field that would be novel and revolutionary by the time I graduate with my Ph.D. Fusing biology, nanotechnology and electromagnetic phenomenon gave me absolute conviction (a very rare event for me) that this is what I wanted to do. For me it was a huge risk to abandon familiar ground and get into something that I had very little idea about, but her faith in my abilities and her support (especially when nothing seems to be working) made my days happier. I always felt that Kim had a genuine concern for my well-being and what was best for me. She never micromanaged and allowed me to make my own mistakes (sorry about the scope), and in my opinion, were pre-requisites to my self-motivation in these past two years.

I want to thank the group of students that I have been surrounded with. I could not have asked for a better group of people to work with. Their support and genuine concern for me made it feel like we were a little family and not just colleagues. Aaron, for our early morning conversations that were definitely off the wall; Victor, for caring for my general well-being despite enduring my stories; Kate, for being a good listener and her take on feminism; Andy, for your Labview program that is the lifeline of the group; Josh, for helping me out with mechanical engineering issues and for spotting me on the labview program; Marie-Eve, for enduring with the amplifier and its ways; Sunho, for very kindly helping me out when I first joined the lab and for interesting conversation; Jordi, for helping me take my mind of things with magic and Diana for her cheeks.

Finally I would like to thank my family for their never ending support and faith in me. Despite having financial problems they would give up everything for my sister and I. Their devotion to the well being of their children always humbles me and reminds of all the times that I disappointed them. For all the oranges that my mom

had to cut up to help me understand fractions and all the times my dad would stay up all night with me to help me study before finals reminds me that there will never be anything that a child can do to compare to all the effort their parents put in for them, I hope that this degree gives back a little.

Contents

List of Figures

List of Tables

Chapter 1

Introduction

Since the dawn of civilization mankind has labored to improve the quality of life by understanding and controlling natural phenomena around him/her. From controlling the destructive nature of fire to power the first steam engines to writing programs that dictate the behavior of welding machines in car factories, man has always looked for a way to automate and simplify dangerous and tedious processes. Up until the 20th century mankind had focused on controlling his/her external world, but with the advancement of knowledge in the biomedical sciences mankind was starting to manipulate internal biochemical processes to help cure diseases. In this process, parallels between the external world of machines and the internal world of biological processes had been drawn up whereby mankind has been striving to control and understand the complex internal processes that not only mimic but has the potential to augment his/her external world.

Cell biology represents the epitome of bottom-up processing technologies where individual processes are specified in detail and are then linked to other processes until a complete system is formed. Cell biology also offers proof that there is at least one existing kind of nanotechnology comprising of devices that carry out numerous functions within living cells . These include using ribosomes to synthesize new proteins according to its DNA code, molecular motors that move components within cells and

even chloroplasts that convert light into chemical fuel. The nascent field of nanotechnology in the 21st century promises to offer unprecedented access and control to the intracellular realm that previously seemed elusive.

Nanoparticles are much smaller than a cell(10-100μm) or a virus(20-450nm) but along the same size of a protein (5-50nm) or a gene (10-100nm long and 2nm wide)[64]. As a result they have been extensively used in medical studies primarily because of their non toxicity, inject ability, biocompatibility and high level of accumulation in target cells[37]. Nanoparticles that have been conjugated with chemical groups that can be recognized by cells, could allow for site-specific drug delivery, especially if the ligand can bind to surface biomarkers [4][13][26][43][14]. These nanoparticles could also help in imaging cells using MRI for early disease detection since they can act as magnetic resonance contrast agents[77][11][22]. It has been demonstrated that iron oxide nanoparticles can be conjugated to arabinogalactan, which is sensitive to the asialoglycoprotein receptors present on normal hepatocytes. [4][6]. It has also been demonstrated that pancreatic cells can be targeted using secretin as a ligand[75]. In addition, it has recently been shown that nanoparticles can also be used to control biomolecular activity [33]. Hamad-Schifferli[33] covalently linked a 1.4nm gold particle to a primary amine in a hairpin loop (molecular beacon) and its absorbance (at 260nm) was observed under the presence and absence of an applied magnetic field as documented in Figure 1-1.

'Induction heating', commonly used in industry to heat macroscopic samples (length scales $\geq 1cm$), is the same method that metallic nanoparticles are used as antennas. When placed in the presence of a electromagnetic field the induced currents in the nanoparticles are converted to heat by the Joule effect. Since biological systems are temperature sensitive this property was recently utilized by Hamad-Schifferli,K. et al.[33] to control DNA dehybridization. Hamad-Schifferli, K. et al. determined that the effective local temperature produced by the nanoparticle was 35^{o}C which

is 13°C above the ambient temperature sufficient to denature proteins and DNA. In addition, the process is entirely reversible since localized heat can be dissipated to the surrounding medium making this technology extremely attractive. However, induction heating is not the only heating mechanism that can be utilized to control biology. Other nanoparticles, ferromagnetic in particular, generate heat predominantly through other relaxation methods rather than induction [42][35][76].

These ferromagnetic nanoparticles were first used by Gilchrist et al.[28][65] in the presence of an alternating magnetic field to heat up micrometer magnetite particles injected into the subserosa of dog intestines. The field of magnetic fluid hyperthermia allows for adequate energy deposition in target cells and not in surrounding bone and other tissue allowing for a highly selective tumor killing system[69][24][54][1][68][61][49] unlike regional hyperthermia [63]. This is highly desirable since some target regions of the body are only accessible by highly invasive methods,e.g., brain tumors[27][25][31] and prostate carcinomas[40].

Generating an alternating magnetic field efficiently is therefore central to this process of controlling biology with the help of nanoscale heat sources. Many authors have documented the frequency and strength of the magnetic field generated by their induction coils [52] but the efficiency of such systems have not been analyzed. This thesis will investigate, theoretically and empirically, the necessary design parameters for an efficient coil necessary for developing the use of nanoparticle heating for biotechnology. Relevant background material will be introduced in chapter 4, followed by theoretical design parameters for induction coils in chapter 5. The experimental setups designed and built are covered in chapter 6 while the results and conclusions are covered in chapters 7 and 8 respectively.

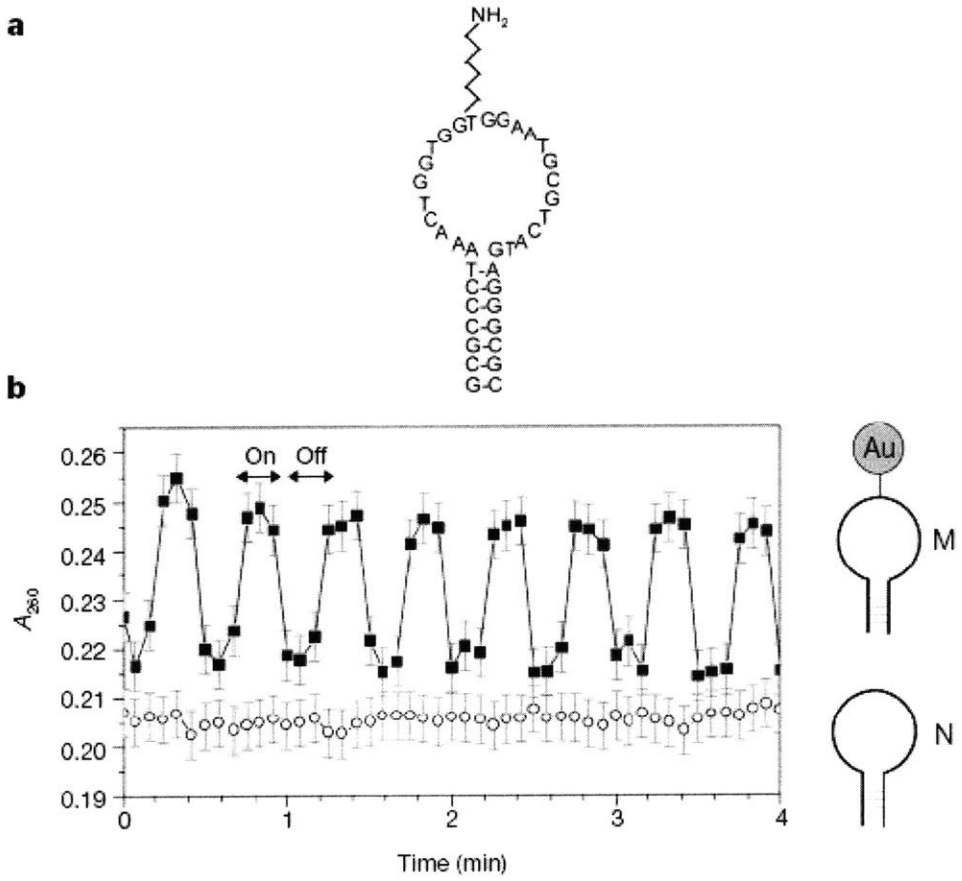

Figure 1-1: Inductive coupling to nanocrystals linked to DNA and evidence of dehybridization. **a**, Sequence of the hairpin molecule,M. The molecule is self-complementary at the ends for 7 bases, with a primary amine in the loop to which a 1.4nm gold nanocrystal is covalently linked. **b**, Absorbance at 260nm (A_{260}) of a solution of M in alternating magnetic fields (squares). Arrows indicate when the alternating magnetic field is on/off. Circles, response of N (no nanocrystals) in alternating magnetic field [33]

1.1 Motivation

The localized heat generated from the low concentrations of nanoparticles has to be maximized to effectively denature the biological species it is attached to. The alternating magnetic flux is the crucial parameter in magnetic nanoparticle heating. It is as a result of this magnetic flux that the nanoparticle undergoes various relaxation schemes to generate heat [42]. There are several different electrical circuit configurations, that can be used to generate a magnetic field, but the easiest way is by using a single-layer coil. This thesis will investigate the design parameters of single-layered coils necessary to optimize the heating of the ferromagnetic nanoparticles.

The devices used to generate the magnetic field are vital in the successful implementation of this method. There are papers that document the details of the coils used in generating the magnetic field necessary for hyperthermia research[76]. They do not, however, discuss the necessary parameters of the coil that would optimize the heating process. This raises the question whether the data obtained is independent of the coil. The reason is partly due to not correlating existing electromagnetic theory with empirical results and as a result not knowing what variables play a key part in optimizing nanoparticle heating. For instance, most authors have been concerned with investigating either the frequency ($\frac{d}{dt}$) or magnetic field strength H independently, rather than from a more physical point of view such as energy supplied (which is proportional to fH^2) . This study will aim to shed light on these concerns.

1.2 Specific Aims of this Study

Until now there has been a very qualitative and empirical understanding of the processes involved in heating nanoparticles. This thesis will plan to "'quantify"' and provide a theoretical backbone for the processes involved.

- This study will investigate this energy approach of heating magnetic nanopar-

ticles.

- Coil parameters necessary to maximize nanoparticle heating.

By achieving these goals this study will help quantify the coil requirements for the magnetic nanoparticle heating system and also will generate results that are not a function of the coil used and only the characteristics of the nanoparticle solution used.

1.3 Background

1.3.1 Nanoparticles

A nanoparticle is a small cluster of atoms(10^2 to 10^3) with a typical size of 1-100 nanometers. Nanoparticles can be metal, dielectric, semiconductor , as well as hybrid structures (e.g., core-shell nanoparticles) that can be grown into various shapes such as nanospheres, nanorods, and nanocups. They are typically used in biomedical applications acting as drug carriers or as quantum dots in quantum information processing[56]. There are also many known techniques for conjugating metal clusters and biomolecules [58]. Multi-dimensional arrays of nanoscale metal clusters can be created by using unique biomolecular characteristics such as DNA hybridization [50][81].

Magnetic material are subject to hysteresis losses where energy is lost during one cycle of changing magnetic field, whereas paramagnetic materials (like gold) have a linear response and are not subject to hysteresis losses. Magnetic nanoparticles sometimes result in single magnetic domains that make them superparamagnetic. This is because the small volume of the nanoparticle allows for its magnetization to be easily affected by thermal fluctuation. Generally tiny magnetic particles are superparamagnetic and empirically Fe_3O_4 particles that are smaller than 10nm in diameter do not have any hysteresis effects. There is, however, experimental evidence

that power losses exist that are comparable with anisotropic particles[16][35][42]. As a result, relaxation processes such as Brownian and Néel are responsible for the heating processes of such particles that do not demonstrate hysteresis losses.

Typical magnetic nanoparticles have a magnetic core (usually magnetite Fe_3O_4, or maghemite -Fe_2O_3) with a biocompatible coating[73][39][4]. Magnetic nanoparticles are non-toxic unlike alternative alternative nanoparticles made of cobalt or nickel. As a result they are the nanoparticles of choice since they can be used for biological applications[38].

1.3.2 Heating Mechanisms

There are essentially two different mechanisms of heating experienced by the nanoparticle in the presence of an alternating magnetic field. Both mechanisms exist in both magnetic and non-magnetic nanoparticles - the extent of the heating is the only difference. Eddy current heating is negligible in small sized particles (< 15nm).

Power Dissipation in Non-magnetic Nanoparticles

Faraday's law of Induction suggests that a change in the magnetic flux generates an electric field and in effect a flow of current in a conductive medium. The resistance to this induced current[32] generates the power loss due to heat.

$$\nabla \times E = -\frac{dB}{dt} \tag{1.1}$$

Faraday's Law with E as the Electric Field and B as the Magnetic Flux Density

The remaining Maxwell's equations help to derive the power lost as heat in the presence of a magnetic field.

$$\nabla \times H = J + \frac{dD}{dt} \tag{1.2}$$

Ampere's Law with H as the Magnetic Field Density, J as the Current Density and D as the Electric Flux Density[45][82]

$$\nabla.B = 0 \tag{1.3}$$

Gauss's law for magnetism with B as the Magnetic Flux Density[45][82]

$$\nabla.D = \rho \tag{1.4}$$

Gauss's law for electricity with D as the Electric Flux Density [45][82]

Equations for power conservation can be derived from Maxwell's equations[7]. This is as follows.

$$\nabla.(E \times H) = H.(\nabla \times E) - E.(\nabla \times H) \tag{1.5}$$

$$\nabla.(E \times H) = H.(-\frac{dB}{dt}) - E.(J + \frac{dD}{dt}) \tag{1.6}$$

$$\nabla.(E \times H) + \frac{d}{dt}\left(\frac{1}{2}\mu H^2 + \frac{1}{2}\epsilon E^2\right) + E.J = 0 \tag{1.7}$$

The final equation expresses the most general energy conservation situation. In that, when energy is supplied to a coil $E.J$ term it is converted into an electromagnetic wave and a magnetic field (The E.J term includes the resistive losses of the coil). It is this magnetic field and electromagnetic wave generated that the nanoparticles get exposed to. Therefore, the sum of the energy density of an electromagnetic wave $\nabla.(E \times H)$ and the energy stored in an electric field and magnetic field $-\frac{d}{dt}\left(\frac{1}{2}\mu H^2 + \frac{1}{2}\epsilon E^2\right)$ should be equal to the loss generated (E.J term) by the nanoparticle with a conductivity σ, dielectric constant of ϵ and magnetic permeability of μ.

The power generated due to eddy current loss can then be determined by taking the volume integral of the square of spatial change in magnetic field strength density (assuming quasistatic approximation for the nanoparticle) divided by the conductivity of the nanoparticle.

$$P = \int \frac{J^2}{\sigma}\, dV = \int \frac{(\nabla \times H)^2}{\sigma}\, dV [82][76] \tag{1.8}$$

Faraday's law suggested that a temporal change was only necessary in generating a current, but the spatial change in magnetic field strength determines the magnitude of the current. The depth from the surface of the particle necessary to drop the magnetic field strength to e^{-1} of its strength at the surface is known as the *skin depth.* The skin depth of a highly conductive material ($\sigma >> \omega\epsilon$) is given by the following equation[45][82][23].

$$d_p = \sqrt{\frac{2}{\omega\mu\sigma}} \tag{1.9}$$

Eq(2.24) suggests that in order to obtain appreciable heating, the frequency of operation should be fairly large to allow for a small skin depth. Typically, the skin depth should be less than half the depth of the penetrating object[17][83].

Power Dissipation in Magnetic Nanoparticles

The first law of thermodynamics suggests that the internal energy for a system of constant density and unit volume (U) is equal to the sum of the heat added (Q) and the work done on the system (W) [72].

$$\delta U = \delta Q + \delta W \tag{1.10}$$

Assuming that no heat is added to the magnetic nanoparticles $\delta Q = 0$ and the only work done is that by the magnetic field ($\delta W = \mathbf{H} \cdot d\mathbf{B}$) The final result is then

$$\delta U = \mathbf{H} \cdot \delta\mathbf{B}[72] \tag{1.11}$$

$\mathbf{H}$ is the magnetic field intensity vector(A m^{-1})
$\mathbf{B}$ is the magnetic flux density vector (T)

The applied magnetic field intensity and the resulting magnetic flux density occur in the same direction, reducing Eq(1.11). to

$$\delta U = H\ \delta B[72] \tag{1.12}$$

where H and B are magnitudes

The general equation for the magnetic flux density B is

$$B = \mu_0 (H + M)\,[82][45] \tag{1.13}$$

where μ_0 is the magnetic permeability of free space ($4\ \pi \times\ 10^{-7}$) and M (A m^{-1}) is the material constant for Magnetization and is a function of the applied field

$$M = \chi H[82][45] \tag{1.14}$$

where χ is the magnetic susceptibility of the material.

Substituting Eq(1.13). into Eq(1.11). and solving for the cyclical increase in internal energy gives

$$\Delta U = -\mu_0 \oint M\ dH \tag{1.15}$$

This equation suggests that magnetic work is converted to internal energy if magnetization lags the applied field. To determine the amount the magnetization lags the applied field requires defining χ as a complex number

$$\chi = \chi^{'} - i\chi^{''}[72] \tag{1.16}$$

If the applied magnetic field is sinusoidal, it can be expressed in the Euler's form as

$$H(t) = Re[H_0 e^{i\omega t}] = H_0 cos(\omega t) \tag{1.17}$$

and the magnetization constant M then becomes

$$M(t) = Re[\chi H_0 e^{i\omega t}] = H_0[\chi^{'} cos(\omega t) + \chi^{''} sin(\omega t)] \tag{1.18}$$

Substituting Eq(1.18) in Eq(1.15) causes the in-phase component ($\chi^{'}$ term) to vanish leaving only the out-of-phase component ($\chi^{''}$ term) of χ.

$$\Delta U = 2\mu_0 H_0^2 \chi^{''} \int_0^{\frac{2\pi}{\omega}} sin^2 \omega t dt \tag{1.19}$$

Eq(1.19) gives the energy converted in one cycle and has to be multiplied by the frequency to get the overall volumetric power dissipation.

$$P = f\Delta U = \mu_0 \pi \chi^{''} f H_0^2 \tag{1.20}$$

With the help of Shliomis's [74] relaxation equation for a motionless magnetic fluid in an alternating field the $\chi^{''}$ term can be related to macroscopic material parameters. In his relaxation equation (Eq(1.21)) M_0 is given as $M_0 = \chi_0 \ H_0 \ cos \ \omega t$ where χ_0 is the macroscopic equilibrium susceptibility.

$$\frac{\delta M(t)}{\delta t} = \frac{1}{\tau}(M_0(t) - M(t)) \tag{1.21}$$

where τ is the relaxation time of the fluid

Substituting Eq(1.18) as M(t) and $M_0 = \chi_0 \ H_0 \ cos \ \omega t$ into Eq(1.21) gives

$$\chi = \frac{\chi_0}{1 + i\omega\tau} = \frac{\chi_0}{1 + (\omega\tau)^2} + i\frac{\omega\tau}{1 + \omega\tau^2}\chi_0 \tag{1.22}$$

Therefore $\chi'' = \frac{\omega\tau}{1+\omega\tau^2}\chi_0$ and can be substituted into Eq(1.20) to give

$$P = \pi\mu_0\chi_0 H_0^2 f \frac{\omega\tau}{1+\omega\tau^2}[72][46] \tag{1.23}$$

There are two types of relaxation processes that the ferrofluid experiences.

1. **Brownian Relaxation** - occurs when the magnetic moment is locked in the crystal axis of the particle, requiring that the particle rotate to align the magnetic moment with the applied field[67].

$$\tau_b = \frac{3\eta V_H}{kT} \tag{1.24}$$

where
η - the viscosity coefficient of the fluid
k - the Boltzmann constant (1.38 x 10^{-23} J K^{-1})
T - absolute temperature (K)
V_H - Hydrodynamic volume of the particle = $\frac{4\pi R^3}{3}(1+\frac{\delta}{R})^3$

2. **Néel Relaxation**[57][76] - at higher frequency brownian motion ceases and a second mechanism (Néel Relaxation) starts to dominate where the magnetic moment within the particle rotates with the applied field.

$$\tau_N = \frac{\sqrt{\pi}}{2}\tau_0 \frac{exp\ \Gamma}{\Gamma^{\frac{1}{2}}} \tag{1.25}$$

$$\Gamma = \kappa \frac{\frac{4\pi R^3}{3}}{kT} \tag{1.26}$$

where
κ - anisotropy constant

A typical ferrofluid can have Brownian and Néel processes going on in parallel, as a result an effective relaxation time can be determined as follows

$$\frac{1}{\tau} = \frac{1}{\tau_b} + \frac{1}{\tau_N} \tag{1.27}$$

and the resulting relaxation constant τ plugged back into Eq(1.23) to obtain accurate power dissipation values.

Magnetic Hysteresis

Hysteresis is well known in ferromagnetic materials. It involves ferromagnetic material absorbing some portion of an external magnetic field such that even when the external field is removed the material remains magnetized. It represents an energy cost for the magnetic dipoles that are 'lagging' with respect to the applied field. In such materials the relationship between magnetic field strength (H) and magnetic flux density (B) is not linear. The relationship between magnetic field strength (H) and magnetic flux density (B) is not linear in such materials. A plot of B against H gives a curve that flattens out with further increase in magnetic field strength. This point where the magnetic field strength results in no further change in flux density is called magnetic saturation.

Similarly reversing the magnetic field gives a similar curve beyond zero flux density but translated from the original curve by an amount known as the remanent flux density or remanence. This translation is due to the fact that ferromagnetic materials tend to retain some of the magnetism induced in them making it a permanent magnet. On the other hand, to bring this magnetization to zero requires a negative coercive field H_c which depends on particle dimension[53]. As a result power loss due to hysteresis depends on both frequency and particle dimension.

Plotting this relationship for all magnetic field strengths results in S shaped loops similar to Figure 1-2. The area of the middle bit of the S represents the work done on the system and represents the heat generated by a ferromagnetic nanoparticle in the presence of an external magnetic field.

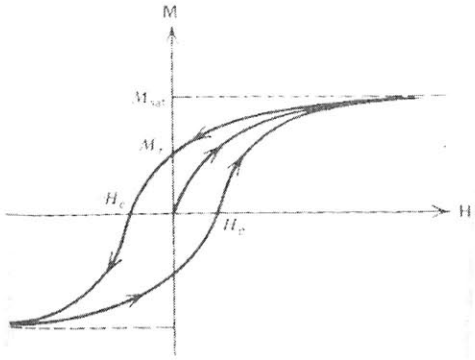

Figure 1-2: Hysteresis in Ferromagnetic Materials[82]

1.3.3 Specific Absorption Rate (SAR)

Specific absorption rate is a method to quantify the mass-normalized rate of RF energy absorption in human tissue [19]. It is commonly adopted in bioelectromagnetics research as a method to quantify the rate of electromagnetic energy deposition in tissue, primarily in in vitro magnetic fluid hyperthermia studies. In such studies, SAR (J $s^{-1}kg^{-1}$ quantifies the amount of energy converted by the magnetic particles in the presence of the magnetic field. This is usually determined from time-dependent calorimetric measurements that measure the rate of temperature rise after applying the magnetic field (as seen in Figure 1-4). The typical experiment setup used to measure SAR (Figure 1-3) typically consists of a sample holder (that is well insulated) placed in the center of a coil while recording temperature changes with a temperature probe. Typical temperature profiles are similar to that of Figure 1-4 with an initial temperature rise till thermal equilibrium is reached (flat part of curve). This is followed by an exponential decay in temperature as soon as the magnetic field is turned off.

Due to the fact that SAR is measured as the initial temperature rise it can be

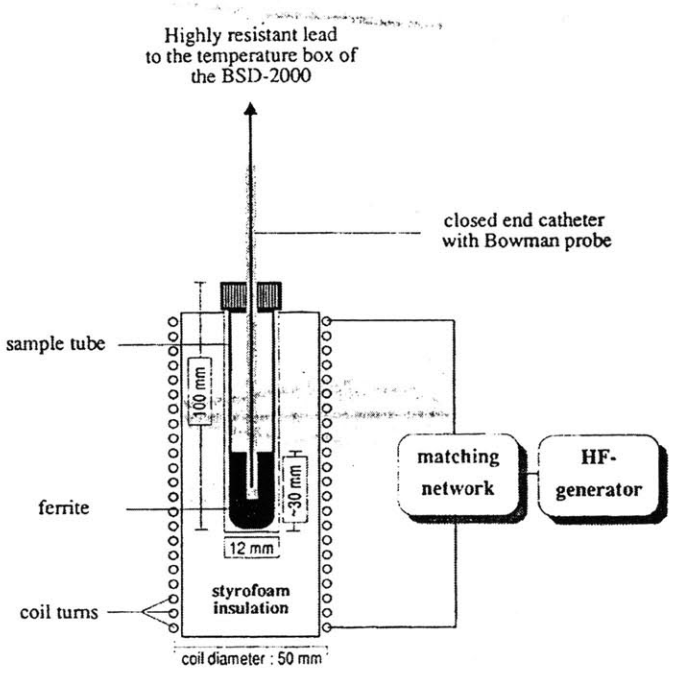

Figure 1-3: Experimental setup for SAR measurements[42]

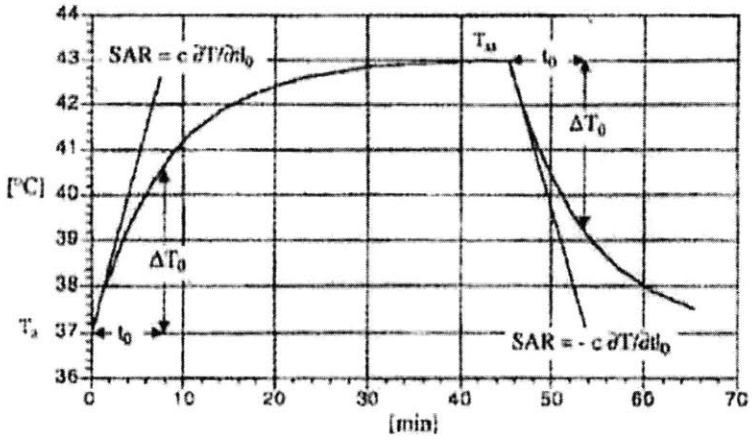

Figure 1-4: Typical temperature profile for SAR Measurements[19]

mathematically expressed as

$$SAR = c\frac{dT}{dt} \tag{1.28}$$

where
c - specific heat capacity of the solution (J kg^{-1} K^{-1}) which is a weighted average of the specific heat capacity of the magnetic particles and solvent
$\frac{dT}{dt}$ - initial rate of temperature rise with respect to time

The previous section described the various methods by which the magnetic particle generates heat. These mechanisms depend on frequency f, magnetic field strength H and material dependent constants κ. SAR should also have a form that describe dependency on such parameters. Empirically SAR is found to be

$$SAR \cong kf^n H^m \tag{1.29}$$

where
k is a frequency-dependent material constant incorporating κ and other parameters

Jordan, A. et al. along with other researchers have [42][35] reported in agreement that the empirical value of m is equal to 2 and n is 1. Although these are empirical results they are based in theory since Eq(1.23) and Eq(1.29) are of the same form (where **k** clumps up many of the terms). Therefore it is only reasonable to think of nanoparticle heating in terms of power delivered and not independent terms of frequency and magnetic field strength.

The Electroquasistatic Regime

Referring back to Eq(1.7), Maxwell's equations have been used to obtain the most general expression for the conservation of electromagnetic power[45][82][18][21][41].

$$\nabla.(E \times H) + \frac{d}{dt}\left(\frac{1}{2}\mu H^2 + \frac{1}{2}\epsilon E^2\right) + E.J = 0 \tag{1.30}$$

Eq(1.30) accounts for the conservation of all power generated by an electrical system. An electrical system that is provided with power will generate an electromagnetic wave ($\nabla.(E \times H)$ term)[10], some resistive losses (E.J term) and will have some energy stored in an electric and magnetic field $\left(\frac{d}{dt}\left(\frac{1}{2}\mu H^2 + \frac{1}{2}\epsilon E^2\right)\right)$.

A coil is commonly known as a device that generates a magnetic field in a region of operation known as the quasistatic regime. When power is supplied to a coil, some is lost in coil resistance, a portion of it is lost as electromagnetic waves and the rest is stored in a magnetic field. The next section proves that Eq(1.30) is still valid despite the fact that the electromagnetic wave generated is neglected in circuit theory.

The foundations of electric circuitry assumes that the quasistatic regime of Maxwell's equations is being obeyed. The assumptions for the electroquasistatic regime are as follows

$$\nabla \times \mathbf{E} = 0 \tag{1.31}$$

$$\nabla.(\epsilon\mathbf{E}) = \rho \tag{1.32}$$

$$\nabla \times \mathbf{H} = \mathbf{J} + \frac{d}{dt}(\epsilon\mathbf{E}) \tag{1.33}$$

The main difference is between the equations of the quasistatic regime and Maxwell's equations is $\nabla \times \mathbf{E} = 0$ which assumes that the time rate of change of magnetic flux does not affect the spatial distribution of the electric field. This is only valid within a certain frequency range, beyond which circuit theory breaks down and alternate methods have to be used.

Assume a characteristic length 'L' and a characteristic time 'τ' and applying it to Ampere's Law and Gauss's law for electricity gives expressions for the exact values of E and H[82].

$$\nabla.\mathbf{E} = \frac{\rho}{\epsilon} \Rightarrow \frac{E}{L} = \frac{\rho}{\epsilon} \tag{1.34}$$

$$E = \frac{\rho L}{\epsilon} \tag{1.35}$$

$$\nabla \times \mathbf{H} = \epsilon \frac{d\mathbf{E}}{dt} \Rightarrow \frac{H}{L} = \frac{\epsilon E}{\tau} \tag{1.36}$$

$$H = \frac{\epsilon E L}{\tau} = \frac{L^2 \rho}{\tau} \tag{1.37}$$

$$\tag{1.38}$$

Determining the actual value of E and the comparing the two Es to obtain the error in this approximation.

$$\nabla \times \mathbf{E}_{actual} = -\mu \frac{d\mathbf{H}}{dt} \tag{1.39}$$

$$\frac{E_{actual}}{L} = \frac{\mu H}{\tau} = \frac{\mu \rho L^3}{\tau} \tag{1.40}$$

$$\frac{E_{actual}}{E} = \frac{\mu \rho L^3 \epsilon}{\tau \rho L} = \frac{\mu \epsilon L^2}{\tau^2} \tag{1.41}$$

$$\frac{E_{actual}}{E} << 1 \Rightarrow \frac{L}{c\tau} << 1 \tag{1.42}$$

where c is the speed of light. This proof suggests that electrical systems can be analyzed using circuit theory if operating in the quasistatic regime - namely the wavelength of operation should not comparable to the characteristic length of the system.In this study, the frequency of operation will enable the coil to be treated as a circuit element.

By setting $\nabla \times \mathbf{E} = 0$ suggests that although an electromagnetic wave is generated (due to the $\frac{dB}{dt}$ term) it hardly affects the entire electrical system and can be ignored. Nevertheless, Maxwell's equations always hold and power supplied to a coil is converted into resistive heat, a magnetic field and a small portion in an electromagnetic wave.

Applying Eq(1.30) to a coil suggests that the magnetic power density stored is expressed by the $\frac{d(\frac{1}{2}\mu H^2)}{dT}$ term. This has uncanny resemblance to Eq(1.29) suggesting that there must be some correlation.

Chapter 2

Coil Requirements

To maximize heating in the nanoparticles most of the power source's power has to be effectively transferred to the nanoparticles. The efficiency of the system should be maximized and one way of accomplishing this is by maximizing the magnetic field generated by the coil. This requires understanding various coil characteristics and honing in on design parameters necessary to maximize heating in the nanoparticles.

2.0.4 Operating Below the Self Resonant Frequency

An ideal inductor is a device that stores magnetic field in an electrical circuit. It is usually denoted by the electrical symbol

A practical inductor, on the other hand, has resistance and capacitance in the turns of the coil ($R_{parasitic}$ and $C_{parasitic}$ respectively) and even inductances and capacitances in the wire leads (L_{lead} and C_{lead} respectively)[23][51][60].

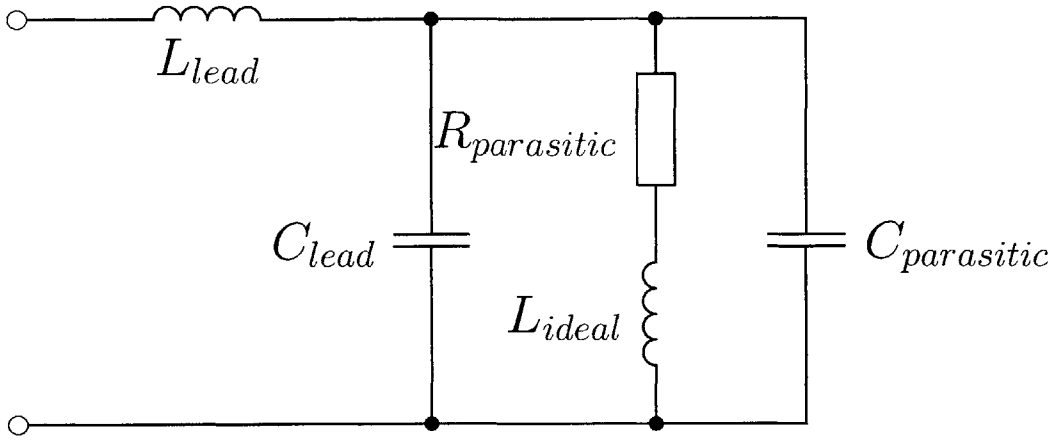

Equivalent Circuit Model for Practical Inductor

The above model may be simplified by assuming that the lead inductances L_{lead} are typically smaller than the ideal inductance L_{ideal} and can be neglected. Similarly, the lead capacitances C_{lead} can also be considered smaller than the capacitances set up between the coil's windings $C_{parasitic}$.

The simplified equivalent circuit model for the inductor now consists of a series combination of $R_{parasitic}$ and L_{ideal} in parallel with $C_{parasitic}$.

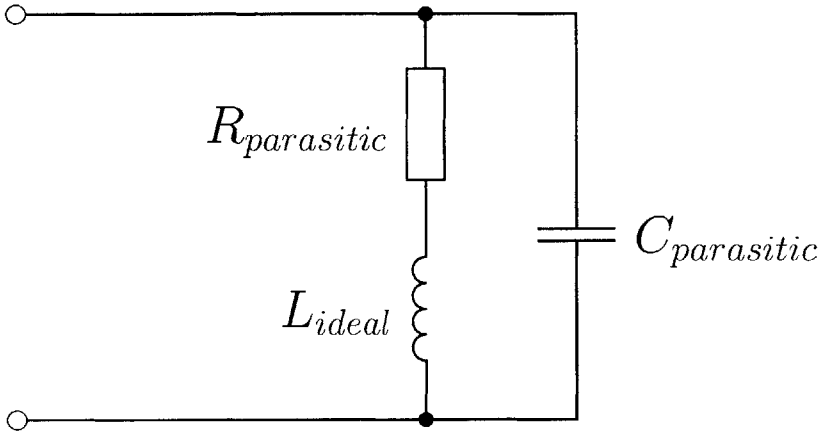

Simplified Equivalent Circuit Model for Inductor

The impedance of this simplified circuit can be written as

$$\frac{1}{Z_{total}} = \frac{1}{Z_1} + \frac{1}{Z_2} \tag{2.1}$$

where

$$Z_1 = \jmath\, \omega L_{ideal} + R_{parasitic} \tag{2.2}$$

and

$$Z_2 = \frac{1}{\jmath\, \omega C_{parasitic}} \tag{2.3}$$

This simplifies to

$$\frac{1}{Z_{total}} = \frac{\jmath\, \omega^2 C_{parasitic} (\jmath\, \omega L_{ideal} + R_{parasitic}) + 1}{\jmath\, \omega L_{ideal} + R_{parasitic}} \tag{2.4}$$

$$Z_{total} = \frac{\jmath\, \omega L + R_{parasitic}}{1 - \omega^2 L C_{parasitic} + \jmath\, \omega C_{parasitic} R_{parasitic}} \tag{2.5}$$

This is the expression for the impedance of an inductor over all frequencies. At low frequencies, the parasitic resistance term dominates and the impedance is approximately $R_{parasitic}$. As the operating frequency increases, the L_{ideal} starts dominating the impedance at

$$\omega = \frac{R_{parasitic}}{L_{ideal}} \tag{2.6}$$

Further increase in frequency, increases the impedance due to L_{ideal} and decreases the impedance due to $C_{parasitic}$. At a specific frequency known as the *self resonant frequency*, the impedance due to the L_{ideal} and $C_{parasitic}$ become equal. The impedance of the overall equivalent model is real and at a maximum at this point. Above the *self resonant frequency*, the $C_{parasitic}$ dominates the equivalent circuit decreasing the

impedance with increasing frequency.

$$w_0 = \frac{1}{\sqrt{LC}} \tag{2.7}$$

Operating below the *self resonant frequency* is the first requirement for an inductor

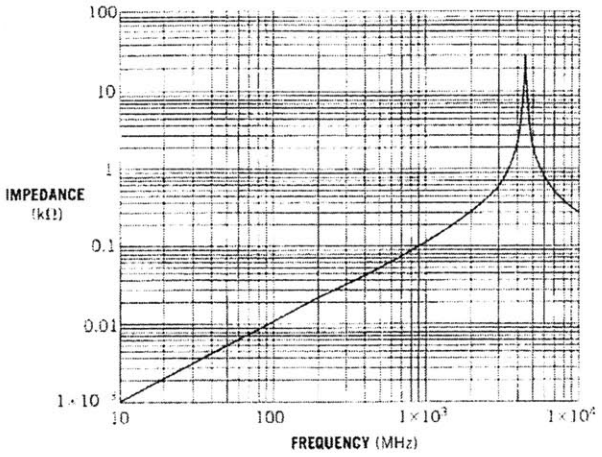

Figure 2-1: Impedance plot of a 0805HQ16N inductor by CoilCraft[23]

used in nanoparticle heating especially since nanoparticle heating has been demonstrated at upto 1GHz.

2.0.5 High Quality Factor

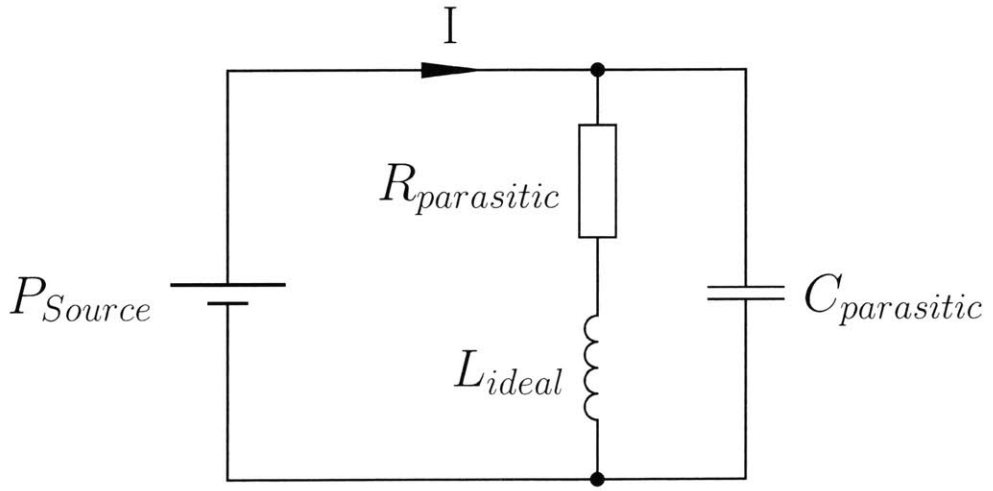

Power supplied by the power source to the simplified inductor model can be given by the relation

$$P = I^2 Z \tag{2.8}$$

Z is the impedance of the inductor model in Eq(2.5) and is a complex number.

$$Z = Z_{real} + \jmath\ Z_{imaginary} \tag{2.9}$$

As a result, the power supplied gets distributed to both the real (resistance) and imaginary (reactance) parts of the impedance.

$$P = I^2 Z_{real} + \jmath\ I^2 Z_{imaginary} \tag{2.10}$$

The real part of the power is the amount of power that is dissipated as heat. This is apparent when a power source is connected to a resistive circuit. All the power from the source is supplied to the resistor which dissipates the power as heat.

Physically, the imaginary part of the power corresponds to the amount of power stored in an electric or magnetic field of the device. Therefore, the power supplied by the source is distributed into the resistive (wasted) portion and the portion where power is stored in an electric/magnetic field. The ratio of the power stored to the power dissipated gives an indication of the 'quality' of the device and is known as the *Quality Factor* (Q)[66][70]. Eq(2.11)can also be considered to be the phase angle of the equivalent model (Θ).

$$Q = \left| \frac{I^2 Z_{imaginary}}{I^2 Z_{real}} \right| = \left| \frac{Z_{imaginary}}{Z_{real}} \right| = \Theta \tag{2.11}$$

Quality factor is often used when dealing with coils used in tuned circuits where the inductance determines the resonance frequency and the sharpness of the tuning depends on 'Q'. The circuit below is an example of a tuned circuit made up of a resistor, inductor and capacitor in series with a sinusoidal voltage source. All passive components are assumed to be ideal.

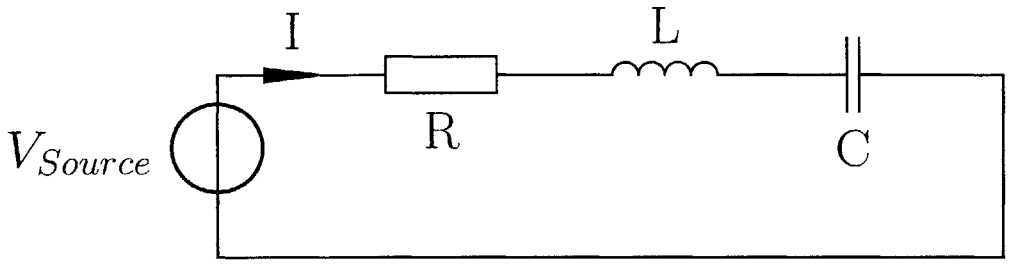

Figure 2-2 is a plot of the magnitude and phase of the transfer function of a typical series RLC circuit. The 'peakiness' of the frequency response curve depends on the ratio of the peak height of the curve to bandwidth at a height of $\frac{1}{\sqrt{2}}$ of the peak height. This ratio is the *Quality Factor* of a resonant tunable circuit.

$$Q = \frac{\omega_0}{|\omega_2 - \omega_1|} \tag{2.12}$$

where ω_0 is the resonant frequency, ω_2 and ω_1 are the two frequencies that correspond to the half-power heights at $\frac{peak}{\sqrt{2}}$.

The phase plot of Figure 2-2 concludes that the equation of Q in Eq(2.11) is the same as Eq(2.12). This implies that the more familiar *Quality Factor* of tuned circuitry and the *Quality Factor* of a passive element share the idea that both are different ways of representing the phase angle of the circuit.

At resonant frequency (ω_0) the tuned circuit and the equivalent inductor model are both resistors having a Quality Factor and phase of 0. Below resonant frequency both circuits are inductive (phase angle is $\frac{\pi}{2}$) where the energy is stored primarily in the magnetic field.

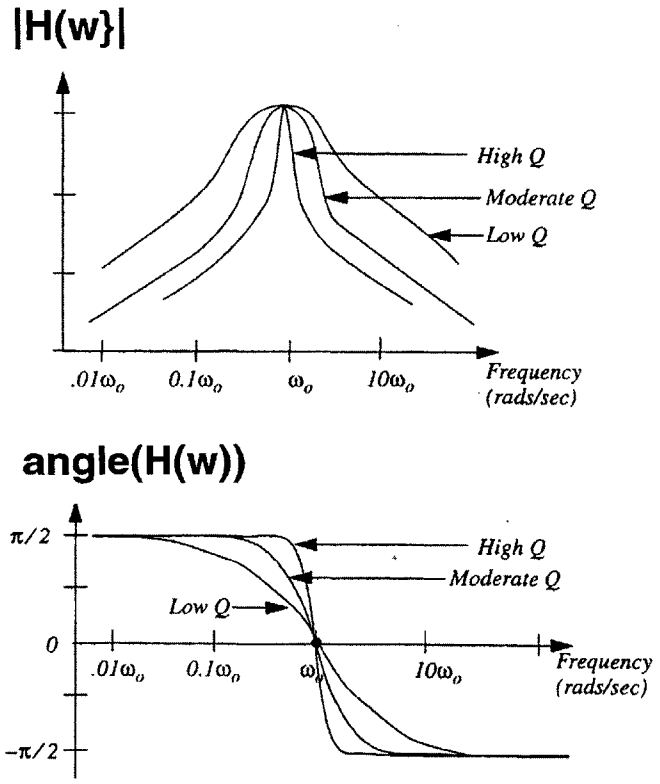

Figure 2-2: Magnitude and Phase plots of High and Low Q series RLC circuits[47]

2.0.6 Designing Coils of High Quality Factor

2.0.7 Types of Coils

There are essentially three families of inductance coils [78].

1. 'Air-cored' Coils

   Coils that have no magnetic material comprising of their core are known to be 'air-cored.'[3][29]

2. Coils with Laminated Iron Cores

   Such coils have cores that are made up of thin sheets of ferro-magnetic materials. These cores are 'stamped out' from large sheets of material and layered with insulating material parallel to the direction of the magnetic flux. This is to

reduce losses due to eddy-currents induced in the core[15][62][71]. The thickness of the laminations depend on the frequency of operation; At higher frequencies the laminations must be made thinner. Leakage flux in the air surrounding the closed-cores are usually assumed to be negligible due to the high magnetic permeability of the core material. Even if an air-gap is introduced, the length of the gap would just reduce the flux density and not affect its distribution.

3. Coils with Dust Cores

   Dust-cores are cores that are made up of compressing a composite material of ferro-magnetic particles coated with an insulating 'binder' material into a uniform mass[48][9][44][79]. As a whole the material will possess magnetic properties that depend upon, but are different from, the particles it is composed. The important property of dust-cores are that they behave similar to gapped-laminated cores. The magnetic flux passes alternately through magnetic particles and the in between non-magnetic gaps forming an effective uniformly distributed 'gap.'[59] This happens even if the material is made into a closed core and the gap-ratio is the ratio between the gap length between adjacent particles and their mean diameter[80].

Of the three families of coils, the air-cored coils have the least material parameters involved and are therefore the easiest to investigate. This thesis will involve the use of air-cored coils but the conclusions of this investigation can be applied to the other coil families and the relevant works are cited.

2.0.8 Air-cored Coils

There are three flavors of 'air-cored' coils. They are

1. Single-Layer Solenoids

   These coils or 'solenoids' are long and thin coils consisting of a single layer of

wire wound such as to minimize the insulating gap between turns.

2. Multilayer Solenoids

   These coils are made by 'layering' the windings on top of each other repeatedly.

3. Toroids

   Coils that are wound in the shape of a torus are known as toroids.

2.0.9 Inductance formulae

Single-Layer Solenoid

The series inductance of such a coil is given by Eq(2.13).

$$L = \frac{4\pi^2 r^2 N^2}{l} 10^{-9} H \tag{2.13}$$

where

N - number of turns
l - length of coil in cm
r - radius in cm

This equation is derived by assuming that the current through the coils are similar to an ideal 'current sheet.' In order for this equation to fit this approximation there should negligible spacing between the turns, strips are used instead of round wires and there is very little fringing so the coil length is much greater than the its diameter. If the coil were to have a length of the same order as its diameter, then a correction factor has to be introduced. The correction factor, known as the Nagaoka constant K_n, is a function of the radius:length ratio and is given in Eq(2.14).

$$K_n = \frac{1}{1 + 0.9\left(\frac{r}{l}\right) - 0.02\left(\frac{r}{l}\right)^2} \tag{2.14}$$

If the turns are spaced far apart and round wire is used, a further correction multiplicative factor Eq(2.17) should be introduced and Eq(2.14) should be multiplied by this factor.

$$Factor = \left[1 - \frac{l(A+B)}{\pi r N K_n}\right] \tag{2.15}$$

$$A = 2.3 \log 1.73 \frac{d}{c} \tag{2.16}$$

$$B = 0.336\left(1 - \frac{2.5}{N} + \frac{3.8}{N^2}\right) \tag{2.17}$$

where

d - diameter (cm) of circular conductor
c - winding pitch

Multilayer Solenoid

The inductance formula of Eq(2.13). can also be applied here because the spacing between the turns is usually small enough to have negligible effect on the inductance. Although the inductance can be determined by the number of turns and the overall dimensions of the windings as in the single-layer case. The Nagaoka constant K_n differs from that of Eq(2.14). and is a function of length, mean radius and depth of windings. Fig(2-3) is a cross-section diagram of a multilayer coil where the depth of windings 't' and the mean radius of r_1 and r_2 are illustrated.

$$K_n = \frac{1}{1 + 0.9\left(\frac{r}{l}\right) + 0.32\left(\frac{t}{l}\right) + 0.84\left(\frac{t}{l}\right)} \tag{2.18}$$

where

t - depth of windings
r - mean radius of coil

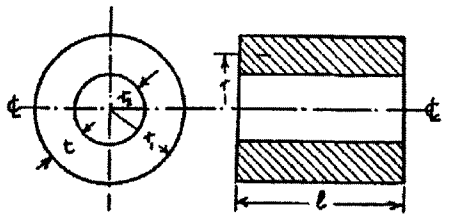

Figure 2-3: Dimensions of multilayer solenoids

Toroids

Fig 2-4(a). is a toroid of small winding depth, whereas fig 2-4(b). is one with deep windings. A critically important ratio is the $\left(\frac{a}{r_0}\right)$. If this ratio is small the inductance

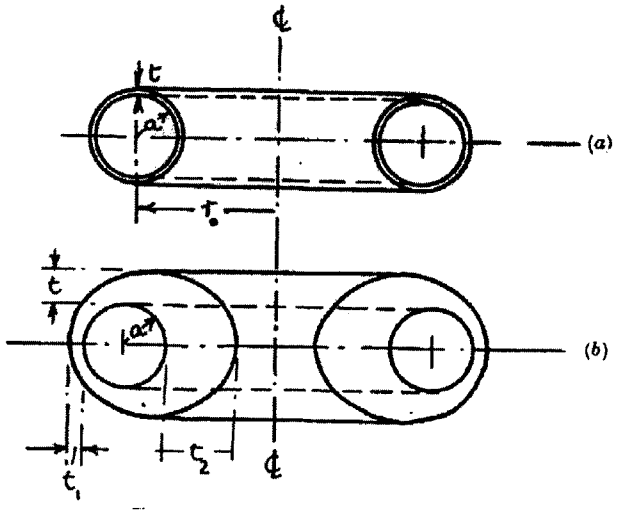

Figure 2-4: Toroid Dimensions

can be accurately estimated to be equal to that of a long solenoid of $r = a$ and $l = 2\pi r_0$.

$$L = 2\pi N^2 r_0 \left(\frac{a}{r_0}\right)^2 10^{-9} H \tag{2.19}$$

The magnetic field intensity distribution over each turn's cross-section starts to no longer become uniform if the ratio $\left(\frac{a}{r_0}\right)$ is increased. An 'effective radius' then replaces the r_0 term and is given as

$$r_{eff} = \frac{r_0}{2}\left[1 + \sqrt{1 - \left(\frac{a}{r_0}\right)^2}\right] \tag{2.20}$$

The inductance is then given as

$$L = \frac{\pi N^2 a^2}{r_0}\left[1 + \sqrt{1 - \left(\frac{a}{r_0}\right)^2}\right]^{-1} 10^{-9} H \tag{2.21}$$

The effective radius deviates very little from the mean radius r_0 even in toroids that do not have circular cross-sections. In general, a fairly accurate method of calculating the inductance of toroids if the cross-sectional area of one turn is known.

$$L = \frac{4\pi N^2 A}{2\pi r_0} 10^{-9} H \tag{2.22}$$

2.0.10 Losses that reduce the Quality Factor

Skin Effect

A conductor carrying an alternating constant amplitude current will generate a constant amplitude alternating magnetic field concentric to the axis of the wire. This field further induces currents, known as 'eddy-currents[8]', within the conductor that dissipates more power than when operating in d.c. These 'eddy-currents' effectively nullify the current and shield it from the magnetic field at the center[5]; while increasing the currents on the surface of the wire. As a result, the current flow not through the entire conductor but rather on a 'skin.' The thickness of this skin gets smaller as the frequency is increased, decreasing the effective area of cross-section increasing the 'resistance' to the flow of current.The resistance of a wire is then proportional to $\frac{\sqrt{f}}{d}$.

Fig(2-5a) illustrates this current distribution in the conductor due to eddy-currents.

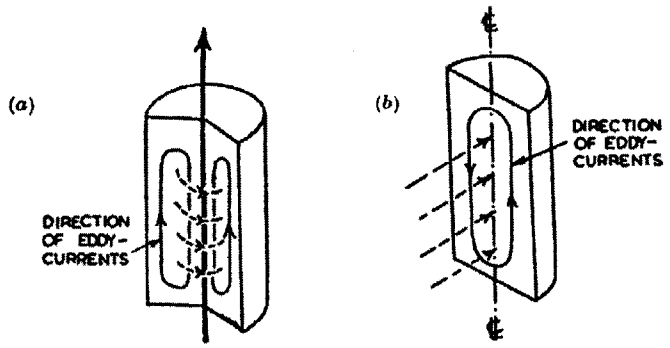

Figure 2-5: Skin effect and Proximity effect in a conductor

'Skin depth' is defined as the radial depth into the conductor from the surface that the magnetic field has dropped to e^{-1} of its value at the surface. The formula for the 'skin depth' can be derived from Maxwell's equations and can be expressed in the form of Eq(2.24) and some typical values are listed in Table (2.1).

$$\delta = \sqrt{\frac{2}{\omega\mu\sigma}} \tag{2.23}$$

$$\delta = \frac{1}{2\pi}\sqrt{\frac{\rho}{\mu f}}10^{4.5}cm \tag{2.24}$$

Material	Depth of Penetration (cm)
Brass	$\frac{12.7}{\sqrt{f}}$
Aluminum	$\frac{8.3}{\sqrt{f}}$
Copper	$\frac{6.6}{\sqrt{f}}$

Table 2.1: Penetration Depth for Common Materials

Infact the a.c. resistance of the wire can be expressed as the d.c. resistance multiplied

by a factor. This factor is a function of the ratio of the diameter of the wire to its skin depth $\left(\frac{d}{\delta}\right)$.

$$R = R_{dc}\,(1 + F) \tag{2.25}$$

where

F - $\left(\frac{d}{\delta}\right)$
R_{dc} - DC resistance of wire

A plot of $(1+F)$ against $\left(\frac{d}{\delta}\right)$, in Fig(2-6). has the factor F negligible since skin effect is not prevalent at low frequencies. At high frequencies $(1+F)$ is seen to become equal to $\frac{1}{4}\left(\frac{d}{\delta}\right)$.

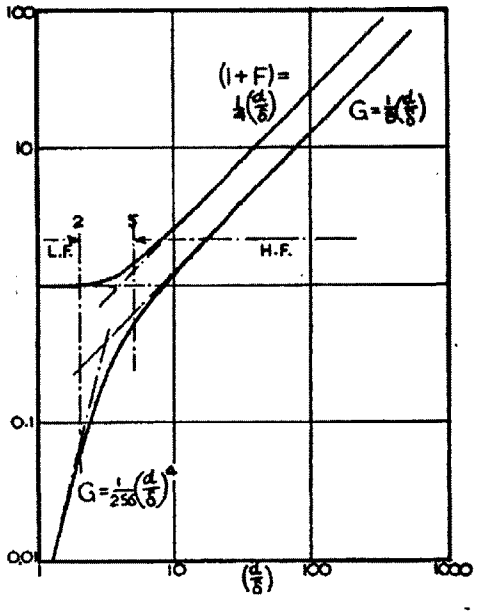

Figure 2-6: Plot of A.C resistance factor $((1 + F))$ against ratio of wire diameter to skin depth $(\left(\frac{d}{\delta}\right))$ necessary calculate skin and proximity-effect losses

Proximity Effect

In addition to skin effect losses, there is also 'resistance' to the flow of current due to the magnetic field generated from neighboring loops of wire. Therefore, at any point in the wire eddy currents are generated due to the magnetic field due to the current in that loop as well as the perpendicular magnetic field due to the current from neighboring loops as in Figure (2-5b). The dominating loss between the skin and proximity effects depends on the number of turns, spacing between the turns and shape of the windings[36]. Eq(2.26). gives the power loss due to a circular wire.

$$P_{loss} = \frac{1}{4} R_{dc} d^2 H^2 G.10^2 Watts \tag{2.26}$$

where

H - r.m.s. magnetic field intensity (A/cm)
G - Numerical factor
d - diameter of wire (cm)

The numerical factor G is dependent on the ratio between the diameter of the wire and the depth of penetration. Figure (2-6b). is a plot of G against $\left(\frac{d}{\delta}\right)$ and helps to indicate two distinct regions. At low frequencies, the value of G equals to $\frac{1}{256}\left(\frac{d}{\delta}\right)^4$ suggesting that the power loss due to the proximity effect is proportional to f^2. At higher frequencies, G is approximately $\frac{1}{8}\left(\frac{d}{\delta}\right)$ and the power loss due to the proximity effect is proportional to $\sqrt{f}$.

Total Power Loss

From Fig(2-6). there are two distinct frequency ranges where eddy-current formulae can be derived.

- At low frequencies losses are mainly due to the proximity effect.
  Losses $\propto f^2 \left[\frac{d}{\delta} < 2\right]$.

The total resistance due to skin and proximity effects is given by Eq(2.27).

$$R = R_{dc}\left(1 + F + \frac{d^2}{c^2}.G\right) \tag{2.27}$$

where

R_{dc} - DC Resistance
d - diameter of wire (cm)
c - distance between loops (cm)

- At high frequencies losses are mainly due to the skin effect and proximity effect both exist.

  Losses $\propto \sqrt{f}.\left[\frac{d}{\delta} > 5\right]$

  If the turns of the coil are not packed close together, the total resistance expression for a single-layer solenoid is given in Eq(2.28)[12], where u is a function of the number of turns and the ratio of the coil length to mean radius. If the turns are packed close together such that $\frac{d}{c}$ is greater than 0.5, Medhurst [55] suggests that Butterworth's results are erroneous and Eq(2.29) should be used.

$$R = R_{dc}\left(1 + F + u\frac{d^2}{c^2}G\right) \tag{2.28}$$

$$R = \frac{1}{4}R_{dc}\left(\frac{d}{\delta}\right)\varphi \tag{2.29}$$

Fig(2-7) of u against $\frac{1}{r}$ gives the appropriate values of u as measured after Butterworth and Fig(2-8). is a plot of φ against $\frac{1}{r}$ for calculating the losses using Medhurst's equation.

An interesting observation using Medhurst's method is the maximum resistance (6 times greater than when straight) is achieved when the coil length is 0.7 times the mean diameter of the coil, mainly due to the 'proximity effect'.

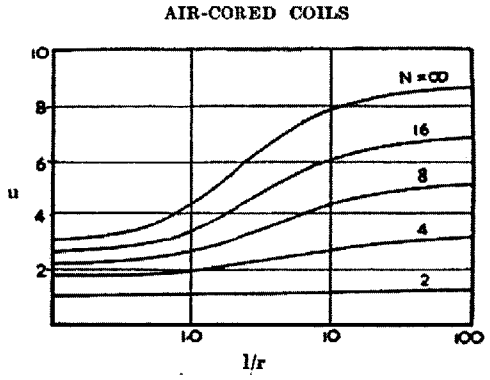

Figure 2-7: Butterworth curves for calculating eddy current losses

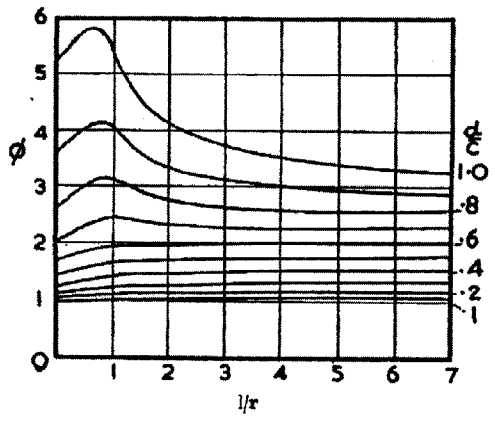

Figure 2-8: Medhurst curves for calculating eddy current losses

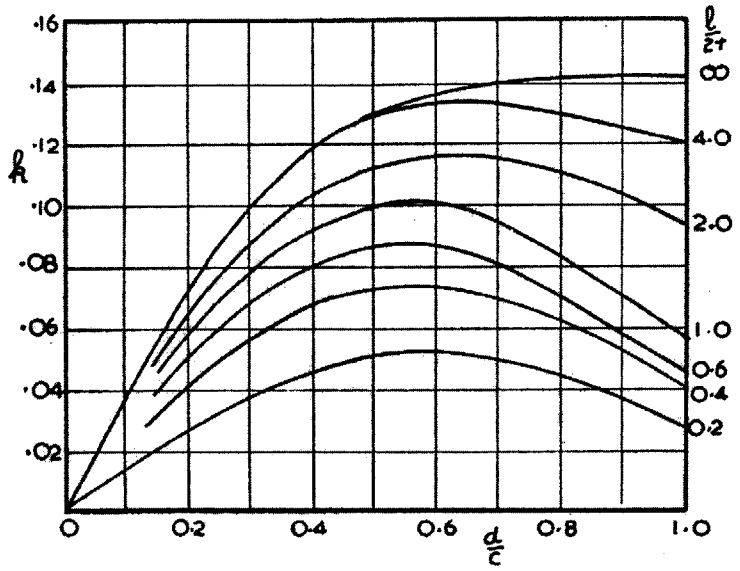

Figure 2-9: Curves relating k to coil spatial relations

2.0.11 Design Considerations for Optimizing Q in Single-Layer Coils

From the previous section the quality factor of a single-layer coil is proportional to $\sqrt{f}$ at high frequencies. The Quality factor is also dependent on the radius of the coil and a spatial factor 'k' and is expressed in Eq (2.30)[34]. Fig(2-9) [55] is a plot of k for various coil dimensions.

$$Q_0 = kr\sqrt{f} \tag{2.30}$$

where

r - mean radius of the coil
k - spatial factor that depends on the $\frac{length}{radius}$ ratio and on relative spacing of turns

Fig(2-9) suggests that, for a given radius and spacing between turns, the maximum Q increases dramatically with increase in coil length till the length equals twice the mean radius. Beyond this length the rate of increase of maximum Q is relatively

smaller.

Two design parameters can be drawn from Fig(2-9) to maximum Q for single layer coils.

1. Optimum spacing between the turns depends on the $\frac{d}{c}$ ratio (diameter to winding pitch). For short coils (length less than twice the radius) $\frac{d}{c}$ should be about 0.55 and can go up to 0.95 for long coils.

2. As the $\frac{d}{c}$ increases, Q decrease. And as $\frac{l}{2r}$ increases the Q increases initially and not so much beyond twice the radius. Welsby suggests that a good compromise is to have $\frac{l}{2r}$ of 1 and $\frac{d}{c}$ of 0.6.

The reason why Welsby suggests using a $\frac{l}{2r}$ may seem arbitrary but has its roots in the self-resonant frequency of the coil. Eq(2.7). suggests that increase in the self-capacitance of the coil turns decreases the self-resonant frequency of the coil, reducing the operating frequency range for the single-layered coil. To maximize the frequency range of operation of the coil the self-capacitance of the turns has to be minimized. Fig(2-10). is a plot used to estimate the self-capacitance of a single layer coil [55]. To keep the self-capacitance to a minimum for a given diameter requires the coil length to be approximately equal to its diameter.

2.0.12 Verifying Welsby's Equations and Design Parameters for High Q Coils

Fortunately Welsby provides an example of single-layer coil design in [78] which can be verified using modern finite element electromagnetic solvers.

> A coil is required to work at a frequency of about 5Mc/sec and is to have an inductance of 20μH. The self-capacitance is to be such that the self-resonant frequency is at least 30 Mc/sec. and the Q at 5 Mc/sec. must not be less than 230.

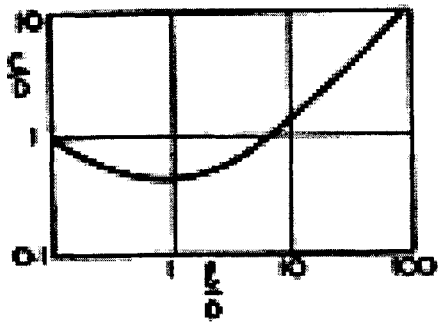

Figure 2-10: Coil Dimensions and Self-Capacitance for Single-Layered Coils. C is capacitance in pF. Coil Length and Capacitance are normalized with respect to Coil Diameter (in cm)

Welsby starts off with his design compromise of having the coil length equal to coil diameter and wire diameter to pitch equal to 0.6. With the help of Fig(2-9)these coil dimensions would give a 'k' of approximately 0.10.Eq(2.30) can then be used to determine a value for the coil radius.

$$r = \frac{Q}{k\sqrt{f}} \tag{2.31}$$

$$r = \frac{230}{0.10\ \sqrt{5}\ 10^3} \tag{2.32}$$

$$r = 1.03cm \tag{2.33}$$

Assuming an upper-estimate of 1pF for the self-capacitance ($\frac{C}{D}$ is less than 1 in Fig(2-10)).The self-resonant frequency ,using Eq(2.7), is determined to be approximately 35MHz. Since this meets the self-resonant frequency requirement ,the self-capacitance is definitely within acceptable bounds.

The next step is to determine the number of turns of coils needed to get an inductance of 20μH.

$$L = \frac{4\pi^2 r^2 N^2 K_n}{l}.10^{-3} \tag{2.34}$$

where

$$K_n = \frac{1}{1 + 0.9\left(\frac{r}{l}\right) - 0.02\left(\frac{r}{l}\right)^2} \tag{2.35}$$

Substituting $\frac{r}{l} = 0.5$ gives..

$$K_n = \frac{1}{1 + 0.45 - 0.005} = 0.69 \tag{2.36}$$

$$L = \frac{2.76\pi 62 r^2 N^2}{l} 10^{-3} \tag{2.37}$$

$$N^2 = \frac{1000Ll}{2.76\pi^2 r^2} = \frac{1000 * 20 * 2.76}{2.76\pi^2 * 1.03^2} \tag{2.38}$$

$$N = 38 \tag{2.39}$$

with a turn pitch of $\frac{2.06}{38} = 0.054$cm and wire diameter of $0.054 * 0.7$=0.038cm. Therefore, a 38 turn coil made of wire diameter 0.038cm and coiled to give a turn pitch of 0.054cm was programmed into the student version of Ansoft's Maxwell electromagnetic solver. The coil was determined to have an inductance of 16.5μH with an error of 6.6%. Despite the value of inductance being slightly off several similar sanity checks were performed giving confidence in the coil design proposed by Welsby.

Coils that operate below the self resonant frequency and have high quality factors should optimize creating the magnetic field necessary for nanoparticle heating. Increasing the quality factor of a coil involves reducing the lossy skin and proximity effects. Welsby has quantified these effects and has drawn up charts to help increase Q for the various coils manufactured today (toroidal, single and multilayer coils).

Chapter 3

Experimental Setup

The experimental setup developed is very similar to that utilized in hyperthermia studies (Figure 1-3 [42]). The basic setup includes a sample holder that is placed in the center of a single-layer solenoid. The coil is placed in an insulated bath that allows for cool water to circulate cooling the coil back down to its initial temperature. The coil is connected to an RF signal generator and amplifier while the current passing through the coil is measured with the help of a current probe. The current allows for the calculation of the magnetic field in the center of the coil. SAR measurements are then made with the help of a temperature probe placed in the sample.

This chapter will document the experimental setup that was developed and used in this study. It will follow a chronological order of the various equipment that was developed to supplement this study.

Apparatus Used

- *RF-immune Temperature probe*

  Most temperature probes utilize metallic components that are easily affected by magnetic fields. A thermocouple for instance, would easily register the incorrect temperature due to eddy currents induced in the probe. The temperature probe needs to sit inside the sample which is being placed inside the coil. There-

fore, this calls for a probe that wont be susceptible to magnetic fields. Fortunately there are a class of temperature probes that are not only flexible and have small dimensions, but are non-metallic and ideal for SAR measurements. *Luxtron®Corp.* manufacture fiber optic probes that have a non-metallic temperature dependent material placed in the tip. Changes in temperature changes the tip's material properties which is detected by the light that is passed down the fiber optic probe.

- *Signal Generator*

  HP 8648D was used

  Specs: Range of operation - (9kHz - 4GHz), Max Power output 0dBm

- *Amplifier*

  Amplifier Research model- 100A250A

  Specs: Range of operation (10Hz - 250MHz), Max Power output 100W

- *Oscilloscope*

  HP 54615B was used

- *Water Chiller*

  Neslab RTE111

- *Current Probe*

  Tektronix AC Current Probe P6022

  Specs: 935 Hz to 120 MHz, 6 A Peak

- *Ferrotec EMG705*

  Ferrofluid manufactured by Ferrotec®consisting of magnetite (Fe_3O_4 of size 10nm and Ms of 220 Gauss) in water with a surfactant.

3.0.13 A Chronology of Setups

The first setup is diagrammatically illustrated in Figure 3-1 with the actual built setup in Figure 3-2. Epoxy was used to make sure that there was a watertight seal and to glue the various pipette bits together. The setup was only intended to demonstrate

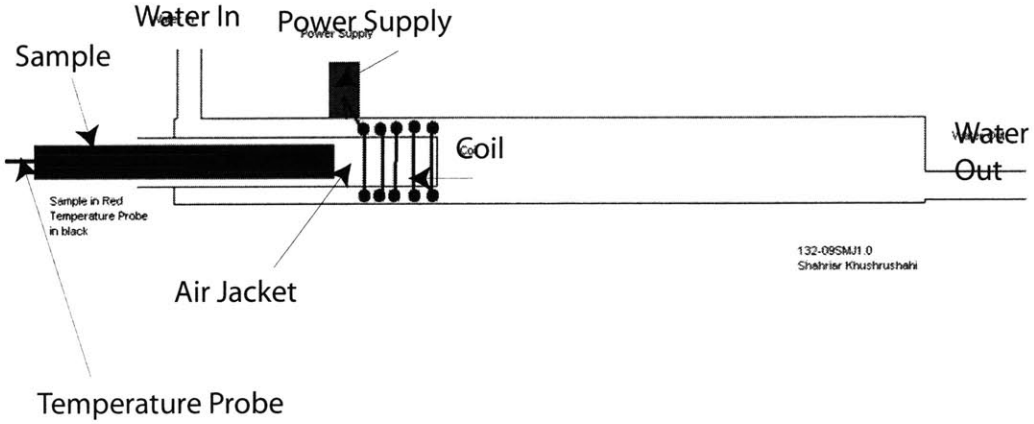

Figure 3-1: Diagram of First Design

heating qualitatively with EMG705. Figure 3-3 illustrates the relative temperature difference between the ferrofluid and that of the water control. It also demonstrates the need for cooling the coil down since the temperature spikes mainly due to resistive heating. The ferrofluid also cools down to the ambient temperature when the power supplied to the coil is stopped. However the design made it difficult to insert the sample so another alternative design was made. Figure 3-4 is the illustration while Figure 3-5 is the actual setup built. The second setup made it easy to insert the sample (tiny glass pipette as seen in Fig 3-5) and results obtained were very convincing that magnetic nanoparticles could heat up to very high temperatures. Until now these were merely setups made to verify the extent to which the nanoparticles would heat with the choice of coils made. Once this was confirmed, there was a need for a setup

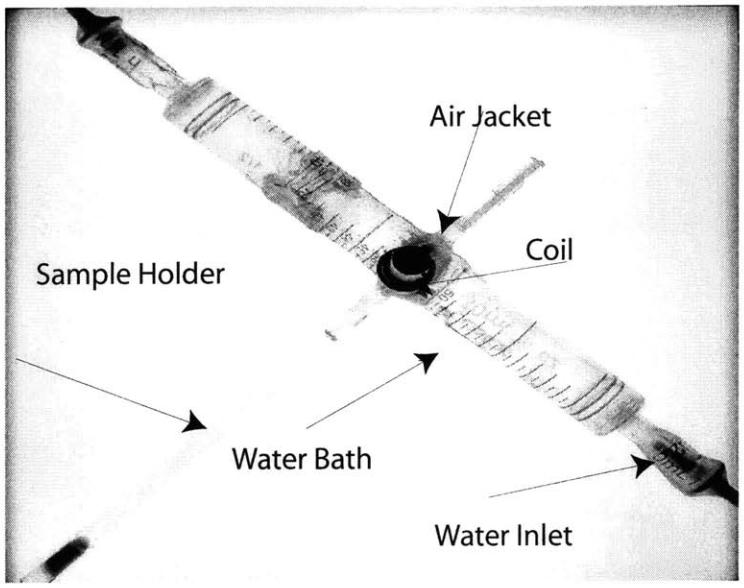

Figure 3-2: Actual Setup

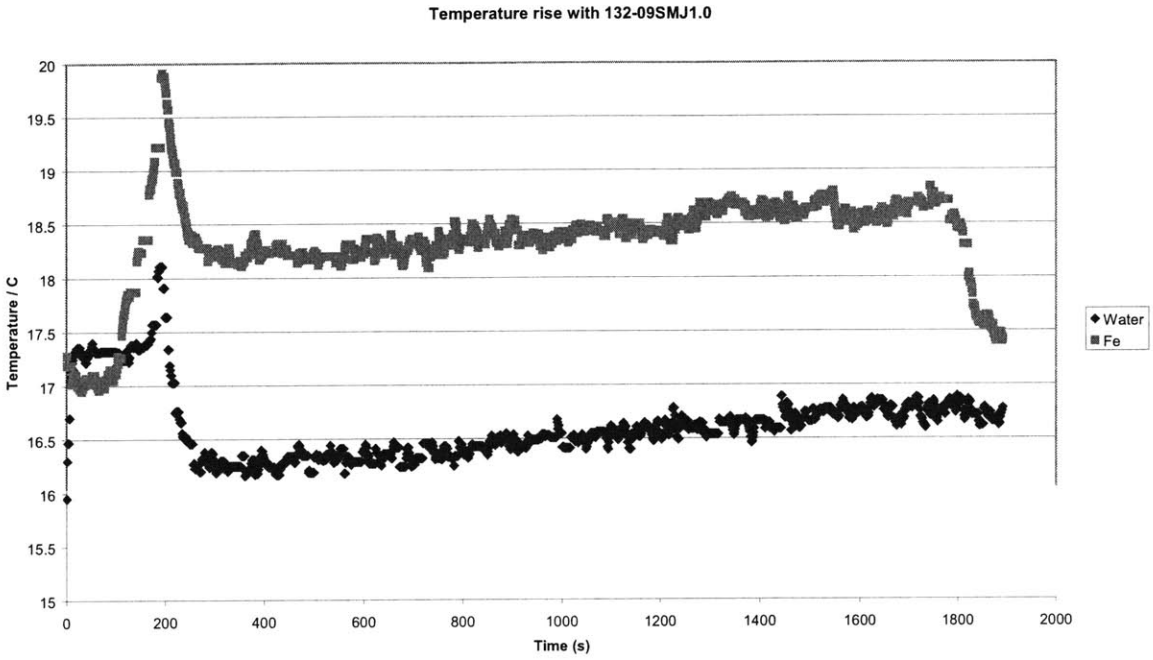
Temperature rise with 132-09SMJ1.0
Temperature / C
Time (s)
Water
Fe
20
19.5
19
18.5
18
17.5
17
16.5
16
15.5
15
0
200
400
600
800
1000
1200
1400
1600
1800
2000

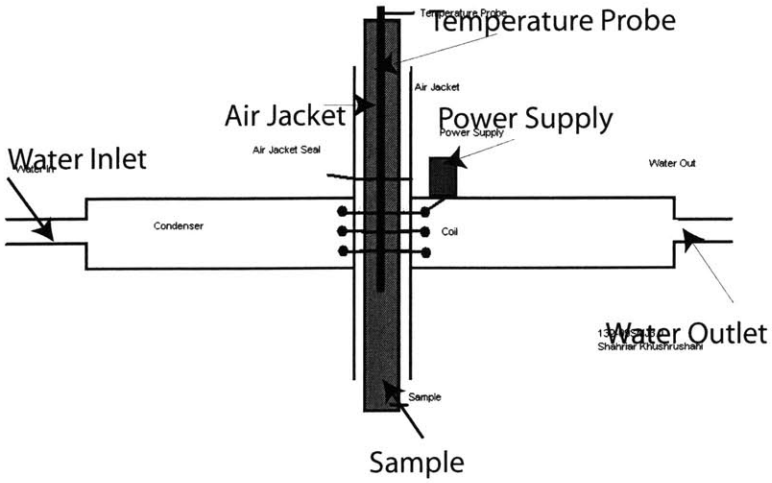

Figure 3-4: Second Design

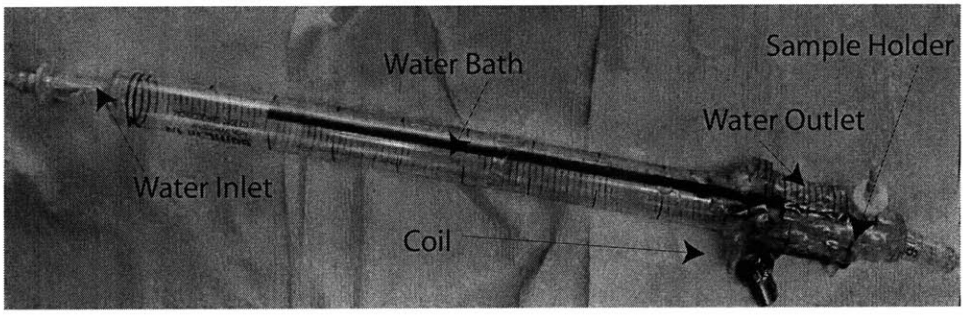

Figure 3-5: Built second design

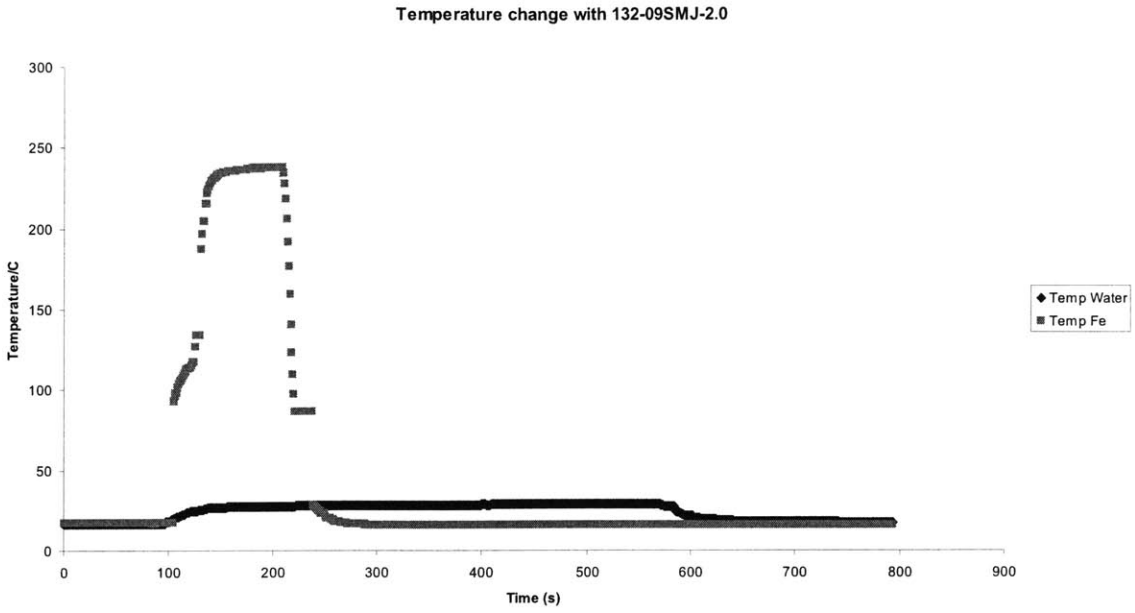
Temperature change with 132-09SMJ-2.0
300
250
200
150
100
50
0
Temperature/C
0
100
200
300
400
500
600
700
800
900
Time (s)
Temp Water
Temp Fe

where it would be easy to change out the coils repeatedly and also allow for the measurement of current through the coil.

Code was written in National Instruments®Labview 7.1 was used to control the signal generator, amplifier and oscilloscope. Labview 7.1 was also the software of choice to code a SAR calculator and other post-processing tools necessary for analyzing results. The third setup allowed for easy change of coils and samples. Figure 3-7 is an external view of the setup. It had plastic pipes that would feed water into the plastic canister. The coil was mounted into the plastic lid and there were leads that would allow for the attachment of the current probe - this is better seen in Figure 3-8 and Figure 3-9. The coil could easily be switched out since the plastic lid could be twisted off the plastic body. Teflon tape was used to ensure that no water leaked from the canister and the coil and the sample holder was the same glass pipette used for the previous designs The problem with the third setup was that it was not electromagnetically shielded. This posed as a serious risk since it would affect the other instruments in the laboratory.

After enough machine skills had been acquired a robust, shielded system was desired that would allow for the easy swapping of coils and samples. The system was designed with the help of Solidworks®. The mechanical drawings drawn up for the coil housing and cooling system (affectionately known as R2D2) are drawn up as follows.

The setup was placed in a EMI shield purchased from McMasterCarr®. The following page documents the technical diagram of such a shield.

The shield was modified to allow for electrical and water connections to R2D2. Holes were drilled to allow for panel mount double-ended female BNC connectors as well as panel mount quick disconnect pipe fittings. The electrical connections utilized modified solderless phono plugs to avoid any wire fracturing due to soldering and repeated assembling and disassembling of setup. Pictures of the modified EMI shield

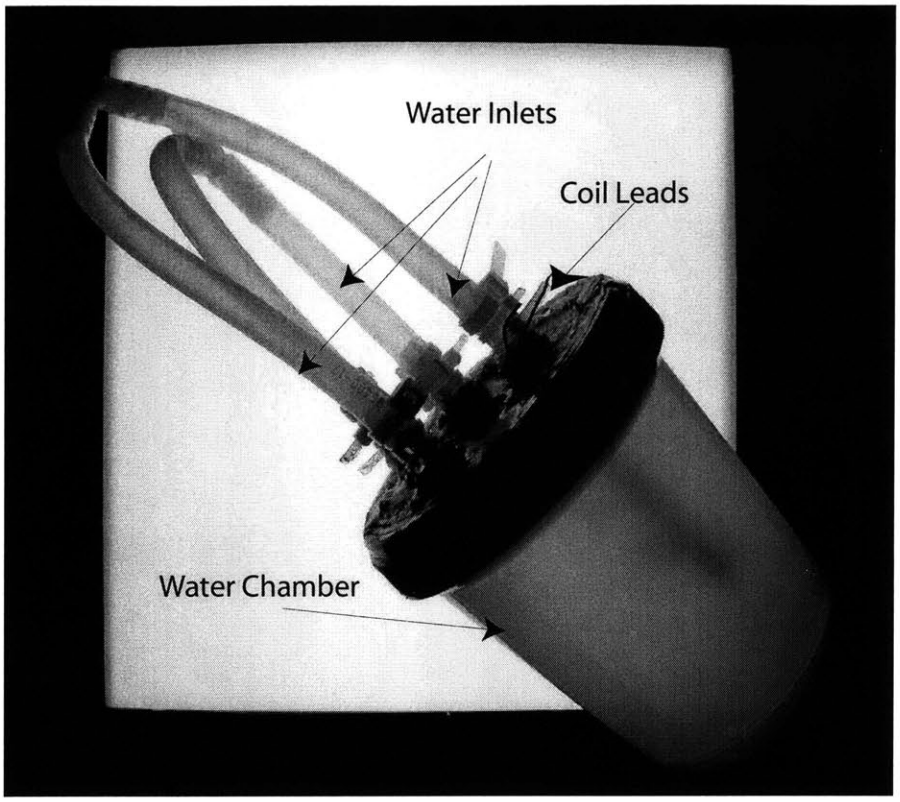

Figure 3-7: External view of the third setup

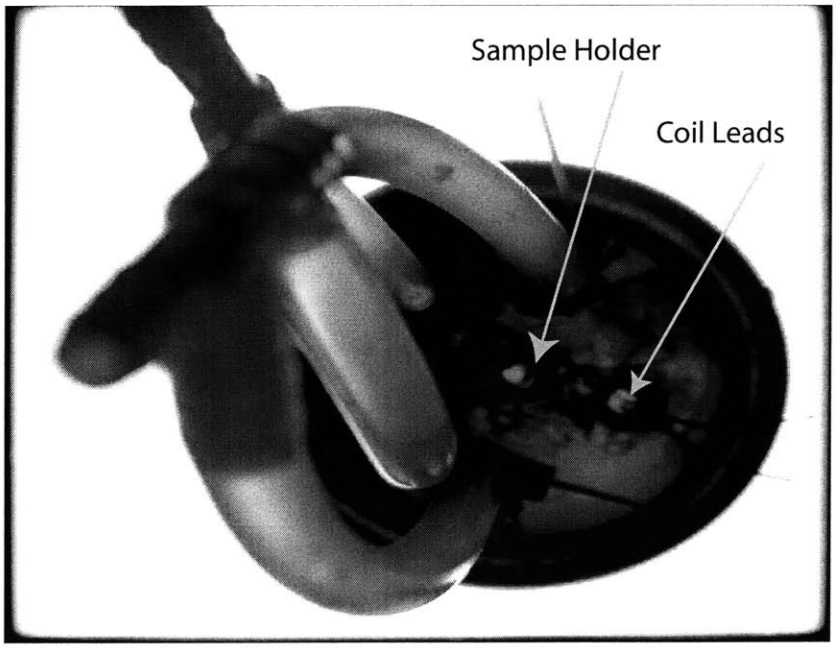

Figure 3-8: Close up on coil leads and sample holder opening

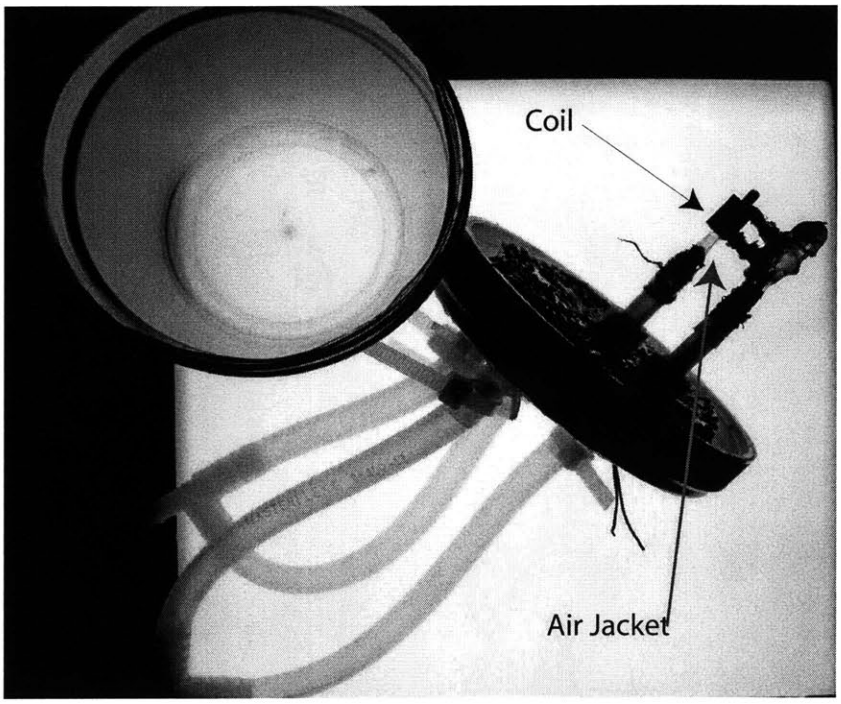

Figure 3-9: Disassembled view of third setup

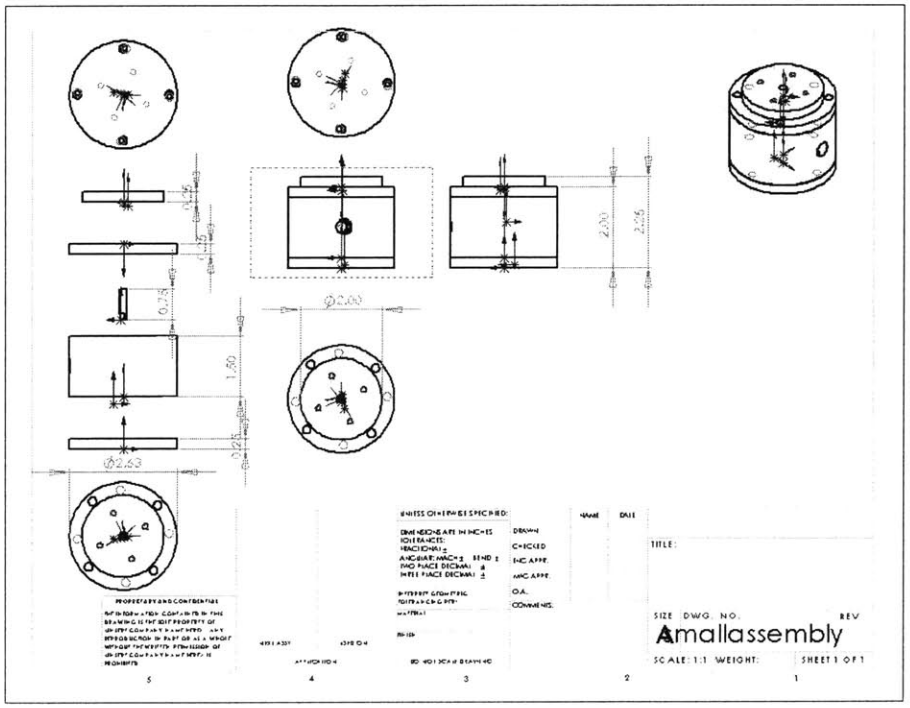

Figure 3-10: Overall Structure of R2D2

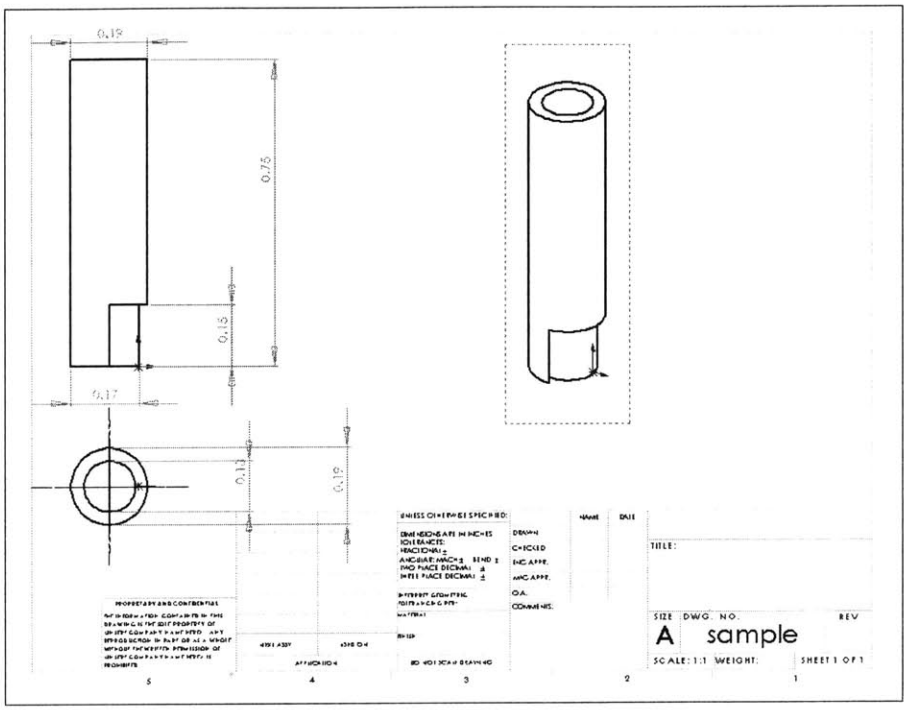

Figure 3-11: Sample Holder for R2D2

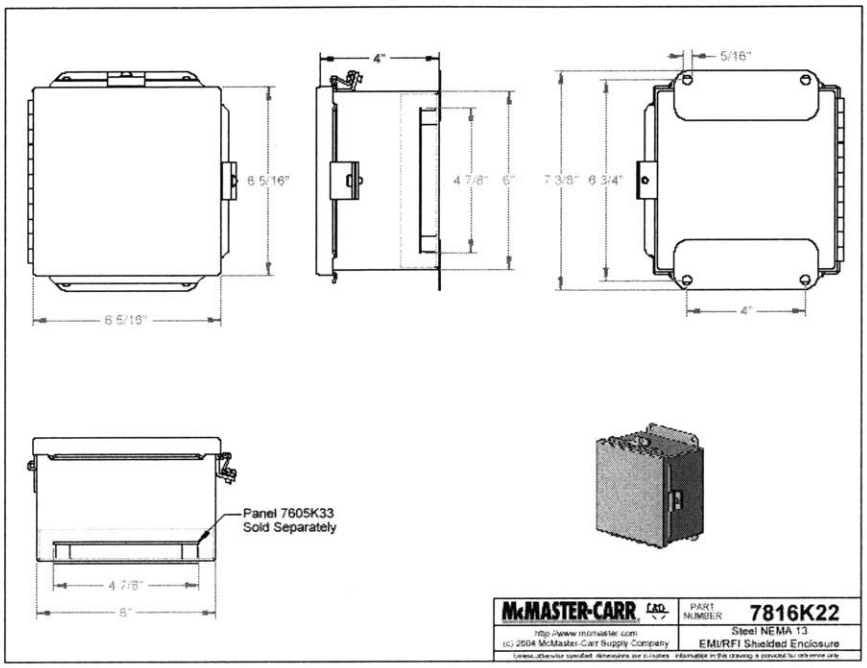

Figure 3-12: EMI Shield

as well as R2D2 and the electrical connections are on the next couple of pages. Figure 3-13 and Figure 3-14 shows the coil setup in its disassembled state and assembled states respectively. All materials (except for the coil and leads) were chosen to be non-metallic to avoid electromagnetic images[2]. Overall, the apparatus built were

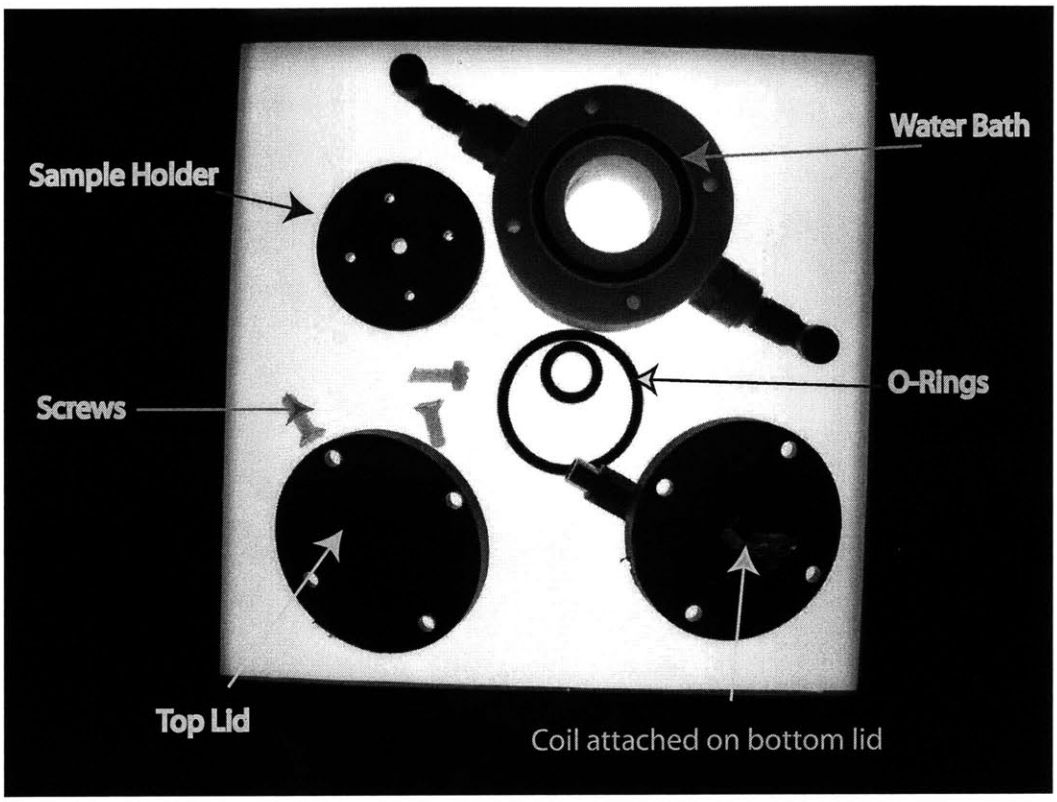

Figure 3-13: Dissasembled R2D2 showing all component parts

similar to those used in hyperthermia studies. The apparatus successfully allowed for rapid cooling of the coil and accurate temperature measurements (due to RF immune probe) allowing for SAR to be measured of the sample by the two different coils.

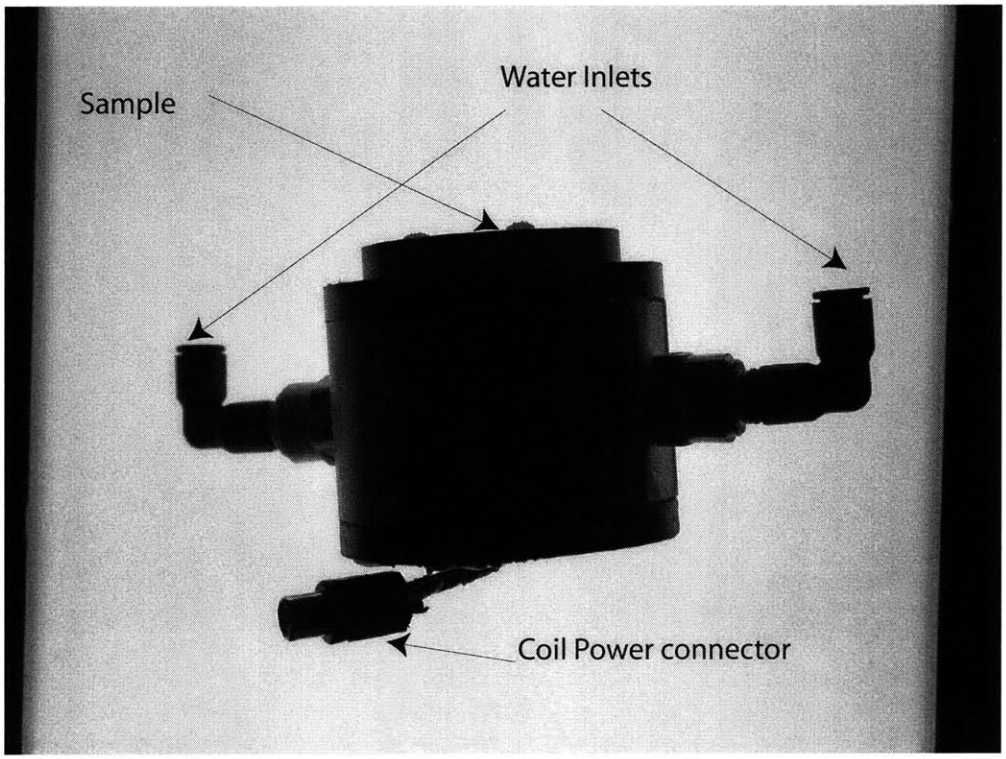

Figure 3-14: Assembled R2D2

Chapter 4

Experimental Results

At first glance, the results suggest that coils with greater quality factors require less energy to heat nanoparticles than those with lower factors. However, when the results proved to be dependent on coil used it suggested that either some theory was overlooked or something was not accurately measured. On further investigation it was realized that transmission line effects due to the coaxial cable were affecting the results obtained.

Two different coils were chosen to heat a solution of ferromagnetic nanoparticles (EMG705 by Ferrotec®) and water. The coils chosen were 132-09SMJ and 132-19SMJ and were manufactured by Coilcraft®. Figure 4-1 below gives plots of Q vs frequency for the two different coils.

An initial test sequence was run at 1MHz intervals from 51MHz to 65MHz. The power applied to the sample was constant at every frequency, requiring values of H to drop as the frequency increased to maintain the product fH^2 constant. Figure 4-2 is a temperature profile plot of water and EMG705 over time for which the sequences in Table 4.1 were applied. Similarly Table 4.2 lists the sequences that were run with the 132-09SMJ coil and Figure 4-3 is the temperature profile plot of water and EMG705 over time. Both plots confirm that the ferromagnetic nanoparticles heat up

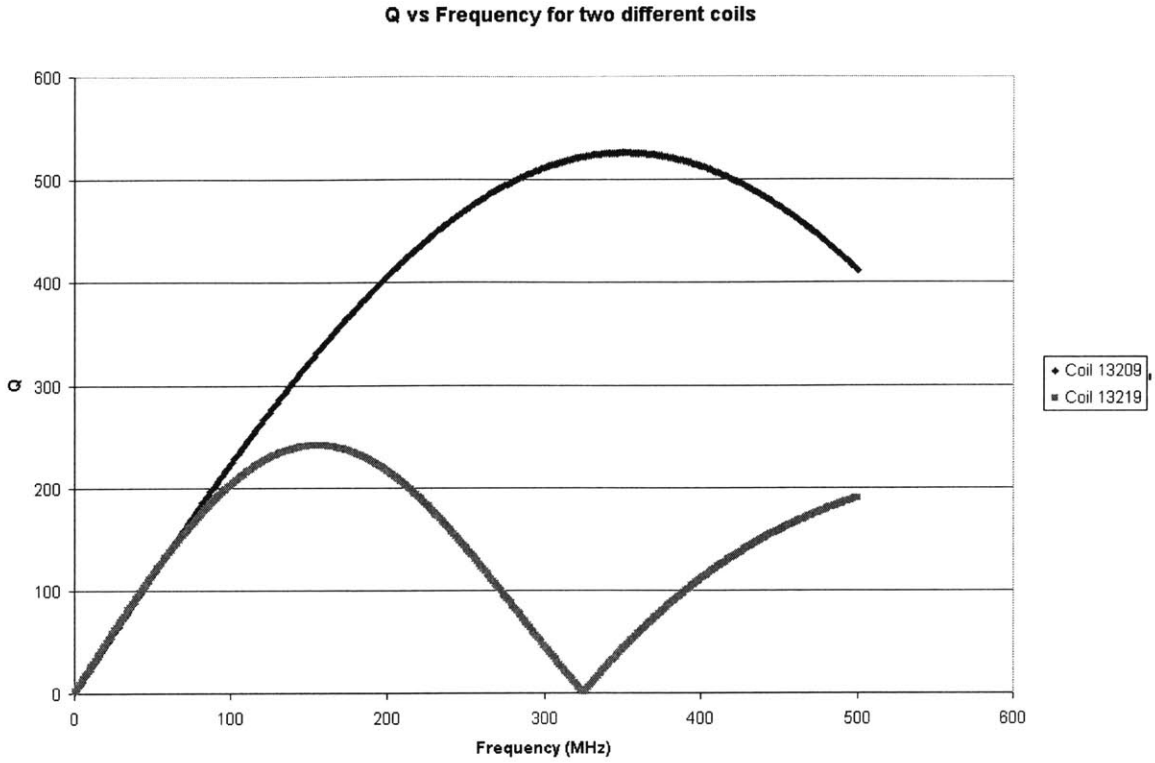

Figure 4-1: Q vs frequency for CoilCraft® coils[20]

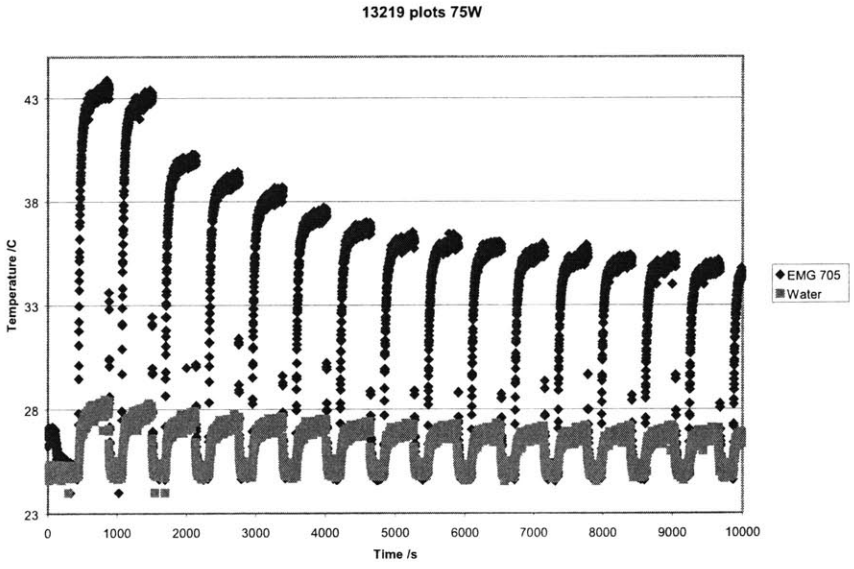

Figure 4-2: Temperature of Water and EMG705 sample using 132-19SMJ coil

Frequency (MHz)	*Magnetic Field Strength H (A/m)*
51	1465
52	1450
53	1437
54	1423
55	1410
56	1398
57	1385
58	1373
59	1362
60	1350
61	1339
62	1328
63	1317
64	1307
65	1297

Table 4.1: Sequences that were run with 132-19SMJ

significantly more than the control solution containing just water.

The two coils had different responses and hence worked with different values of fH^2. There is a suspicion that dielectric heating is the primary cause of the heating in the water and not resistive heating. This makes it difficult to relatively compare the results obtained. Thompson et al. uses a circuit approach to ferromagnetic heating. Using this method it is possible to estimate the extra energy needed for the coil to reach the same Magnetic Flux Density (H). This assumes that the ferromagnetic sample has a greater resistance (R_s) than plain water (this is because the ferromagnetic sample is made of ferromagnetic particles suspended in water). By obtaining and normalizing the gains of the amplifier (Table 4.3) it is possible to compare the efficiency of the coils.

$$P_{sample} = N^2 I^2 Z_{coil+sample} \tag{4.1}$$

$$P_{water} = N^2 I^2 Z_{coil+water} \tag{4.2}$$

$$\frac{P_{sample} - P_{water}}{P_{water}} = \frac{R_{sample} - R_{water}}{R_{water}} \tag{4.3}$$

Frequency (MHz)	*Magnetic Field Strength H (A/m)*
51	846
52	837
53	829
54	821
55	814
56	807
57	800
58	793
59	786
60	780
61	773
62	767
63	761
64	755
65	749

Table 4.2: Sequences that were run with 132-09SMJ

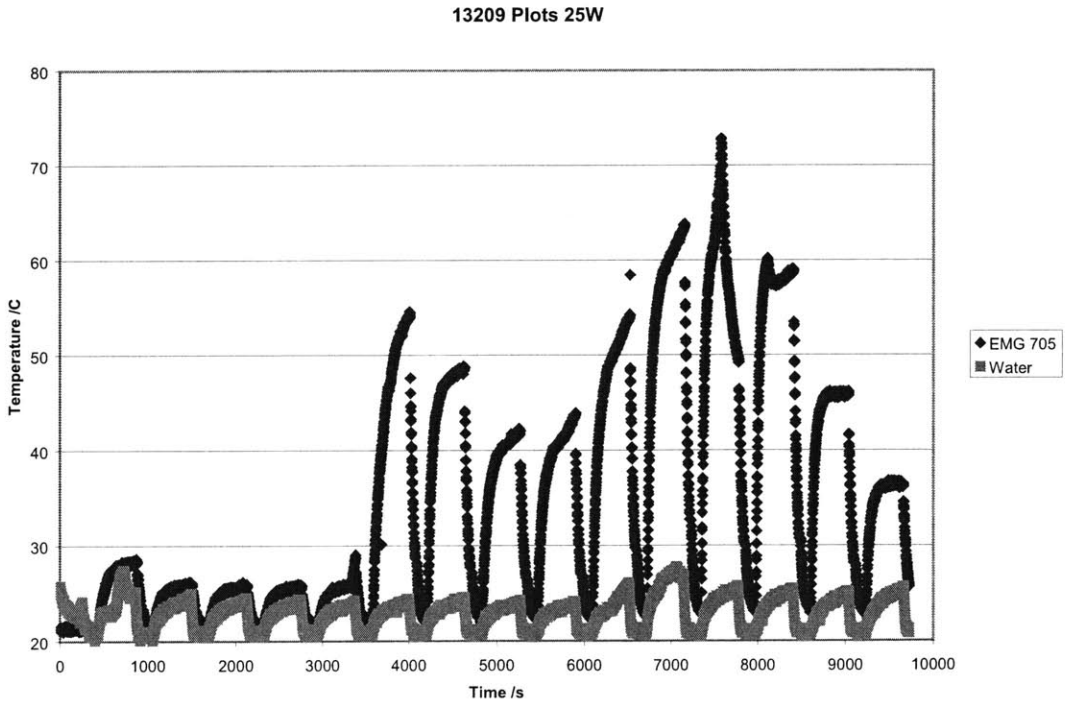

Figure 4-3: Temperature of Water and EMG705 sample using 132-09SMJ coil

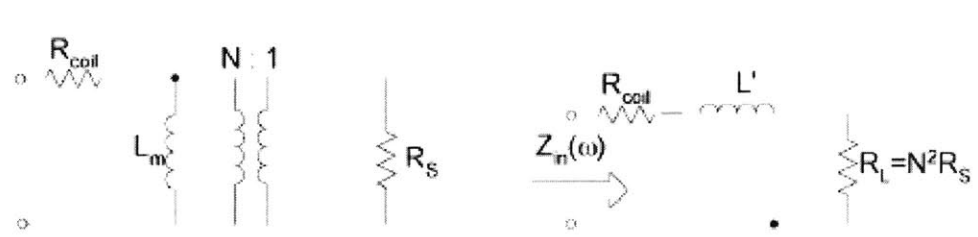

Figure 4-4: Lumped circuit model of heating mechanism [76]

f (MHz)	*132-09 H_2O*	*132-09 EMG705*	*132-19 H_2O*	*132-19 EMG705*
51	3869	3901	1739	1982
52	3862	3891	1587	1737
53	3784	3830	1515	1659
54	3679	3671	1524	1580
55	3564	3556	1423	1444
56	3488	3484	1282	1321
57	3429	3427	1167	1185
58	3332	3325	1060	1138
59	3250	3236	1004	1099
60	3160	3146	1000	1069
61	3069	3056	1031	1099
62	2983	2965	1108	1170
63	2972	2952	1202	1276
64	2839	2885	1341	1366
65	2799	2772	1558	1531

Table 4.3: Gain Tables for 13209 and 13219

Normalizing the power gets rid of the heating dependence on the number of turns of the coil. It also removes the fH^2 dependence since the current dependence is removed when normalized. This should give some indication of the efficiency of the different coils utilized. Figure 4-5 suggests that 132-09SMJ requires less energy than 132-

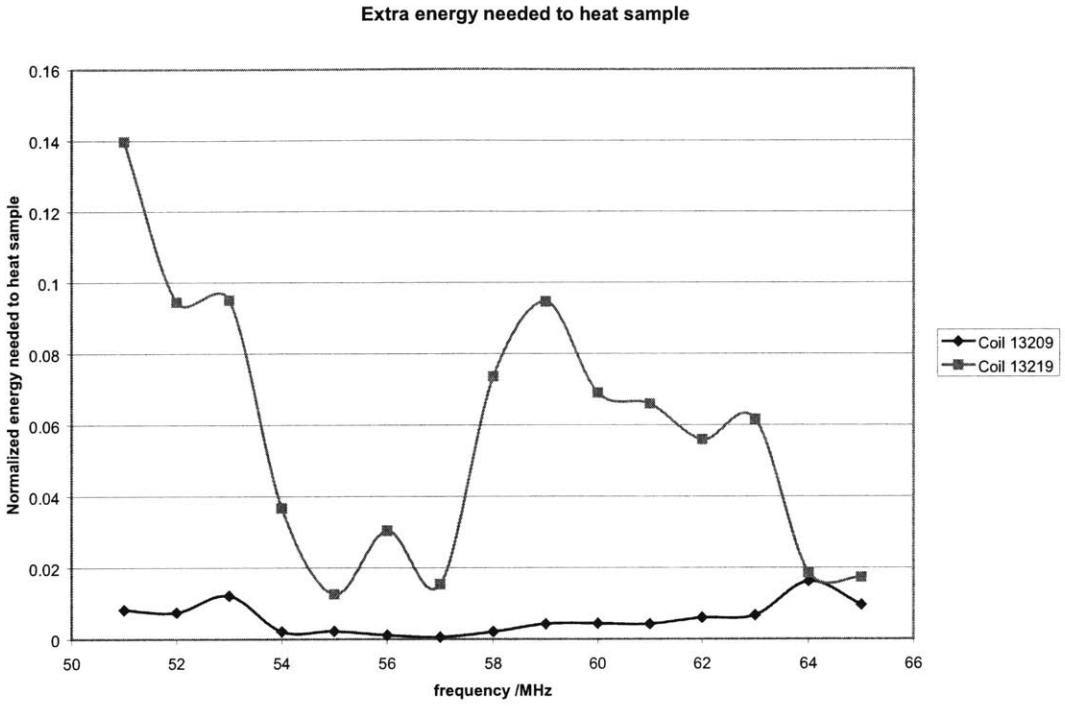

Figure 4-5: Extra energy required by coils to heat sample

19SMJ to heat up the nanoparticles. Verifying this with an enlarged portion (Figure 4-6) of the Q plot suggests that although the difference in Q is tiny 132-09SMJ is a better coil than 132-19SMJ. When values of SAR were determined for the different coils and were normalized the results (Figure 4-7) for the different coils did not follow the Q plots as expected. This meant either something was wrong with the theory involved or the data was being collected incorrectly.

Transmission Line effects have hindered the results of these experiments. Further

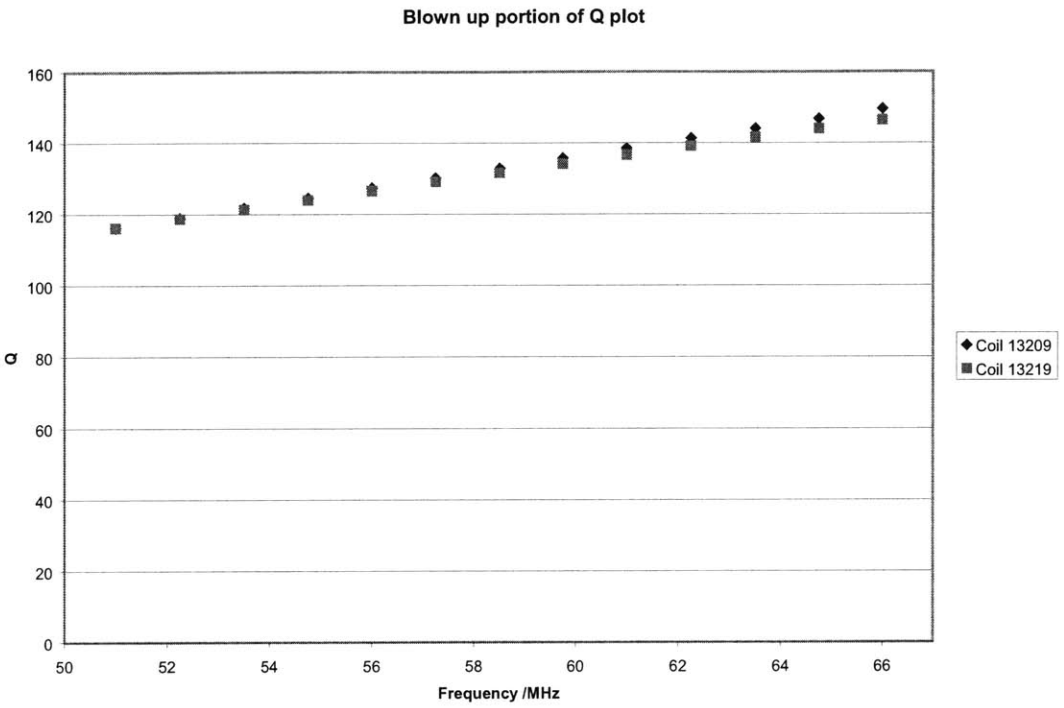

Figure 4-6: Blown up section of Q plot[20]

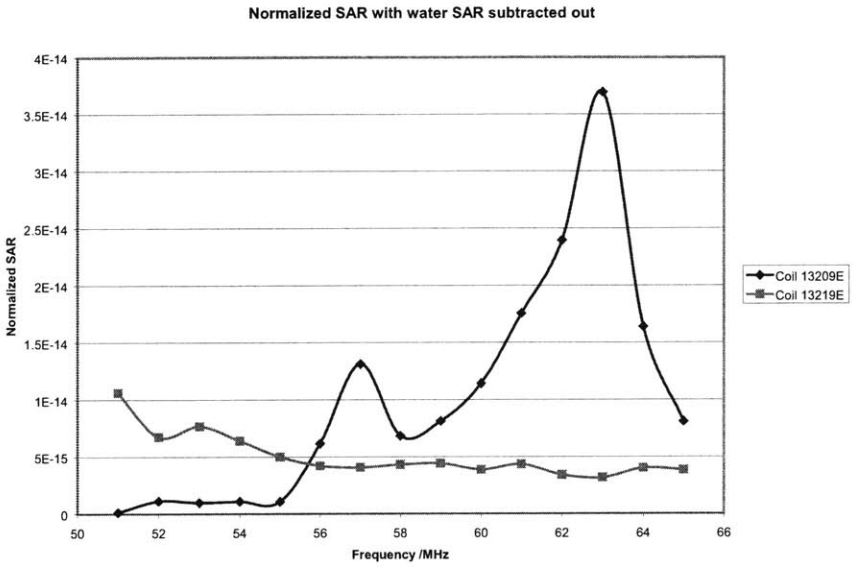

Figure 4-7: Normalized SAR of data from the different coils

investigation suggested that inconsistent results were being obtained from the current probe. It would give different readings of current at different locations on the wire and in different orientations. Although the coil was operating in the electroquasistatic regime the coaxial cables, utilized in making the connection to the coil, suggested that the change in current along the cable shows a considerable change. This raises into question the results obtained particularly since different cable lengths (affecting results obtained) were possibly used every time the apparatus was setup.

Although the results obtained are probably not useful since transmission line effects would mean that the current through the coil and magnetic field was not constant as it was hoped to be. However, if the system were to be impedance matched to allow for minimal transmission line effects, the current experimental setup should deliver the results as expected. In addition, it could be possible to predict nanoparticle heating behavior given device parameters of the coil. If the inductor can have its characteristics lumped into parameters that involve resistors, capacitors and inductors; it would suggest that nanoparticle heating normalized with coil characteristics could also be predicted. However, the old model for inductors predicts an error of only 1% if operating at a frequency $f = \frac{SRF}{10}$ [30]. Considering that the classical function of inductors, as electrical circuit components, would not challenge the old inductor model brings into question whether it is valid at all for high frequency applications.

4.0.14 Failure of the old model

The old model is applicable up to an arbitrary frequency equal to SRF/5. The equations that help describe the impedance of the old model can be manipulated to determine that the peak Q occurs at a frequency equal to $\frac{SRF}{\sqrt{3}}$ [30]. This value does not compare to that quoted by inductor manufacturers. Typically values of Q peak lower than the $\sqrt{3}$ factor by a range of factors from 2 to 50 but values of 3 to 10 are typical [30].

Another reason why this model fails miserably at high frequencies is that it cannot predict Q behavior beyond the self resonant frequency. The imaginary part of the impedance increases monotonically with frequency beyond the self resonant frequency, subsequently blowing up Q. This could be remedied by adding a resistor in series with the capacitor since it would lower the Q at high frequencies above the self-resonant frequency and would also allow for adjusting the peak Q frequency (Figure 4-8). However, Leslie suggests that the model is not robust enough and there are significant difference between measured and predicted Q values [30]. Leslie suggests having both

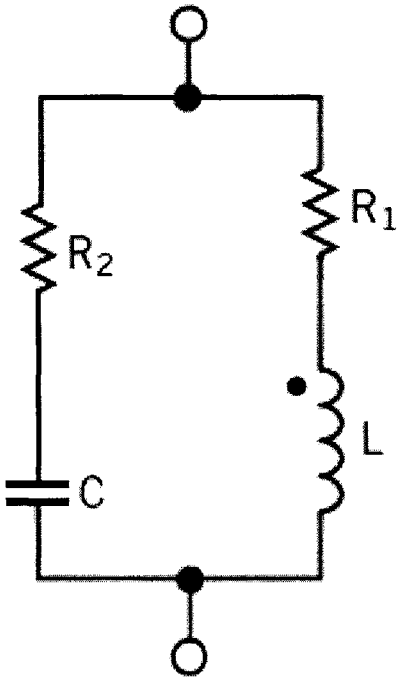

Figure 4-8: Model improved by adding a series resistor with the capacitor

shunt and series resistors for a better inductor model. The series resistor gives a Q that increases with frequency whereas that in parallel gives a Q that decreases with frequency. The combination allows for the peak Q frequency to be adjusted. The new model that Leslie suggests allows for simple equations which can be solved to

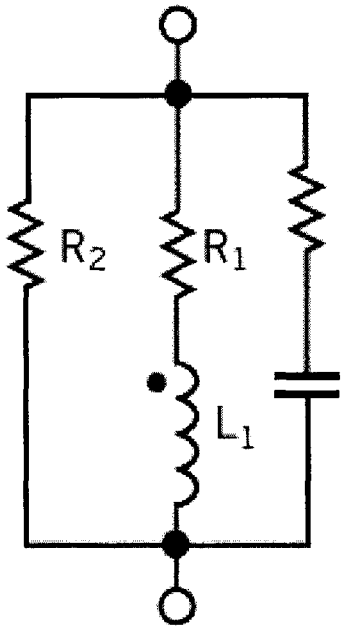

Figure 4-9: The better model for inductors

find particular circuit elements.

$$Q_{max} = \frac{1}{2}\sqrt{\frac{R_2}{R_1}} \tag{4.4}$$

$$f_{Q(max)} = \frac{\sqrt{R_1 R_2}}{2\pi L} \tag{4.5}$$

Given the value for the peak Q and the frequency it occurs at the resistor values can be easily determined.

$$R_1 = \frac{2\pi f_{Q(max)} L}{2Q_{max}} \tag{4.6}$$

$$R_2 = 2Q_{max} \times 2\pi f_{Q(max)} L \tag{4.7}$$

Leslie [30] then goes on to relate the resistors to actual physical characteristics of the inductor.

$$R_1 = K\sqrt{f} = R_s(\frac{f}{SRF})^{\eta} \tag{4.8}$$

The series loss resistance of the inductor (R_1) is typically given by $K\sqrt{f}$ but Leslie suggests that normalizing the loss resistance to the self resonant frequency is more accurate. Hence R_s is the series loss resistance and η should be between 0.5 and 1. He prescribes an iterative procedure that would help derive the correct component values for the model

- Inductor is set to the low frequency inductance value
- Capacitance is set to 15% higher than the manufacturers' minimum SRF data

$$C = \frac{1}{(2\pi SRF)^2 \times L} \tag{4.9}$$

- The resistor in series with the capacitor is set to 1Ω and $\eta = 0.5$. R_s should

then be adjusted till the peak Q is approximately correct.

- If the peak Q frequency is not correct - the SRF can be changed by adjusting the capacitance or by changing the value of the resistor in series with the capacitor (a higher value will lower the peak Q frequency).

- Repeat the process of moving the peak Q frequency and adjusting the peak Q amplitude until it matches that of the data sheet.

- Adjusting the loss-correction term η helps to modify the values of Q leading up to the peak. Large values of η raises the low-frequency values and slightly lowers the peak Q frequency.

By adjusting these values an accurate model for an inductor can be derived and consequently its effect on nanoparticle heating can also be theoretically determined.

Overall, even though the data obtained requires adjustment due to transmission line effects. The theory behind it is sound and the experimental setup has already proven that SAR measurements can be easily and accurately made. By eliminating transmission line effects, the results that will be obtained will open the door to further analysis and discovery. It should also be possible to allow for theoretical determination of nanoparticle heating given device parameters.

Bibliography

[1] Klaus Maier-Hauff Manfred Johannsen Peter Wust Jacek Nadobny Hermann Schirra Helmut Schmidt Serdar Deger Stefan Loening et al. Andreas Jordan, Regina Scholz. Presentation of a new magnetic field therapy system for the treatment of human solid tumors with magnetic fluid hyperthermia. *Journal of Magnetism and Magnetic Materials*, 225:118–126, 2001.

[2] P.R. Bannister. The image theory for electromagnetic fields of a horizontal electric dipole in the preence of a conducting half space. *Radio Sci.*, 17:1095–1102, 1982.

[3] R.T. Beatty. Design of air-gapped chokes. *Wireless Engineer*, page 61, February 1934.

[4] C. C. Berry. *Journal of Materials Chemistry*, 15(5):543–547, 2005.

[5] A.G. Bogle. Inductance and resistance of screened coils. *Journal of the Institution of Electrical Engineers*, page 299, September 1940.

[6] B. Bonnemain. *J. Drug Targeting*, 6:167, 1998.

[7] H.G. Booker. *Energy in Electromagnetism.* Peter Peregrinus, New York, 1982.

[8] H. Buchholz. Eddy-current losses in wires. *Archiv fur Elektroechnik*, page 360, 1929.

[9] S.E. Buckley. Nickel-iron alloy dust-cores. *Electrical Communications*, page 126, June 1948.

[10] K.G. Budden. *The Propagation of Radio Waves.* Cambridge Univ. Press, 1985.

[11] Trevor; Witwer Brian; Zhang Su-Chun; Strable Erica; Lewis Bobbi K.; Zywicke Holly; Miller Brad; van Gelderen Peter; Moskowitz Bruce M.; Duncan Lan D.; Frank Joseph A. Bulte, Jeff W. M.; Douglas. *Nature Biotechnology*, 19(12):1141–1147, 2001.

[12] Butterworth. *Experimental Wireless*, 3:203.

[13] S. Wells M. J. Dalby C. C. Berry, S. Charles and A. S. S. Curtis. *Int. J. Pharm.*, 269:211, 2004.

[14] I. K. Paark S. H. Kim M. Uchiyama C. S. Cho, K. Y. Cho and T. Akaike. *J. Controlled Release*, 77(7):1, 2001.

[15] W. Cauer. Effective permeability and iron losses in sheets and wires. *Archiv fur Elektrotechnik*, page 308, 1925-6.

[16] Kirpotin D.B. Chan, D.C.F. and P.A.B. Jr. Synthesis and evaluation of colloidal magnetic iron oxides for the site specific radiofrequency-induced hyperthermia of cancer. *Int.J.Hyperthermia*, 122:374–378, 1993.

[17] G. Chen. Nanoscale energy transport and conversion: A parallel treatment of electrons,molecules,phonons and photons (in press).

[18] D.K. Cheng. *Field and Wave Electromagnetics.* Addison-Wesley, MA, 1983.

[19] C. K. Chou. Use of heating rate and specific absorption rate in the hyperthermia clinic. *International journal of hyperthermia: the official journal of European Society for Hyperthermic Oncology, North American Hyperthermia Group,*

6(2):367–70, 1990. ENGLAND ISSN: 0265-6736; NLM Unique Journal Identifier: 8508395 English Grant Number: CA33572; Grant Info: CA; Agency: NCI Index Medicus Journal Article.

[20] CoilCraft. *Maxi Spring Air Core Inductors*, 2005.

[21] D. Corson and P.Lorrain. *Electromagnetic Waves and Fields.* Freeman, San Francisco, 1962.

[22] L. Josephson D. Hogemann, V. Ntziachristos and R. Weissleder. *Bioconjugate Chem*, 13:116, 2002.

[23] R.K Feeney and D.R Hertling. *Introduction to RF and Microwave Design.* Georgia Institute of Technology, Georgia, 1998.

[24] S.B. Field and J.W. Hand. *An Introduction to the Practical Aspects of Clinical Hyperthermia.* Taylor and Francis, New York, 1990.

[25] Harsh G. *Brain Tumors.* Churchill Livingstone, Edinburgh, 1995.

[26] X. Yu P. M. Winter K. K. Karukstis M. J. Scott R. W. Fuhrhop D. E. Scherrer G. M. Lanza, D. R. Abendschein and S. A. Wickline. *Acad. Radiol.*, 9:S330, 2003.

[27] in: A.H. Kaye E.R. Laws (Eds.) G.G. Giles, M.F. Gonzales. *Brain Tumors.* Churchill Livingstone, Edinburgh, 1995.

[28] R.K. et al Gilchrist. Effects of electromagnetic heating on internal viscera: a preliminary to the treatment of human tumors. *Annals of Surgery*, 161:890–896, 1965.

[29] E.V.D. Glazier. The inductor with air-gaped magnetic circuit. *Engineering*, 148:406.

[30] Leslie Green. Rf-inductor modeling for the 21st century. *EDN*, September 27,2001 2001.

[31] McDermott M W; Sneed P K; Gutin P H. *Seminars in surgical oncology*, 14(1):79–87, Jan-Feb 1998.

[32] D.J. Hagemaier. *Fundamentals of Eddy Current Testing.* The American Society for Nondestructive Testing Inc., Columbus, OH, 1990.

[33] Kimberly Hamad-Schifferli, John J. Schwartz, Aaron T. Santos, Shuguang Zhang, and Joseph M. Jacobson. Remote electronic control of dna hybridization through inductive coupling to an attached metal nanocrystal antenna. *Nature*, 415(6868):152, 2002. 02046837138 Compilation and indexing terms, Copyright 2005 Elsevier Engineering Information, Inc. 0028-0836 Biomolecules.

[34] C.R. Hanna. Design of air-gapped chokes. *Journal of the American Institution of Electrical Engineers*, page 128, 1927.

[35] Rudolf Hergt, Wilfried Andrae, Carl G. d'Ambly, Ingrid Hilger, Werner A. Kaiser, Uwe Richter, and Hans-Georg Schmidt. Physical limits of hyperthermia using magnetite fine particles. *IEEE Transactions on Magnetics*, 34(5 pt 2):3745, 1998. 98104411253 Compilation and indexing terms, Copyright 2005 Elsevier Engineering Information, Inc. 0018-9464 Magnetite fine particles Magnetic hysteresis losses.

[36] H. Inuma. Measurement of high-frequency resistance of oscillatory circuit. *Proceedings of the American Institution of Radio Engineers*, page 467, Mar. 1931.

[37] Masashige; Honda Hiroyuki; Kobayashi Takeshi Ito, Akira; Shinkai. Medical application of functionalized magnetic nanoparticles. *Journal of Bioscience and Bioengineering*, 100(1):112–115, 2005.

[38] M. Rutnakornpituk J. Connolly, T. G. St Pierre and J. S. Riffle. *Eur. Cells Mater*, 3:106, 2002.

[39] S. A. Gomez-Lopera R. C. Plaza J. L. Arias, V. Gallardo and A. V. Delgado. *J. Controlled Release*, 77:309, 2000.

[40] S.A. Loening et al. J.A. Paulus, R.D. Tucker. *J. Endourol*, 11:225, 1997.

[41] J.D. Jackson. *Classical Electrodynamics.* Wiley, New York, 1962.

[42] A. Jordan, P. Wust, H. Fähling, W. John, A. Hinz, and R. Felix. Inductive heating of ferrimagnetic particles and magnetic fluids: physical evaluation of their potential for hyperthermia. *International journal of hyperthermia: the official journal of European Society for Hyperthermic Oncology, North American Hyperthermia Group*, 9(1):51–68, 1993. ENGLAND ISSN: 0265-6736; NLM Unique Journal Identifier: 8508395 English Index Medicus Journal Article.

[43] Y. Kawashima. *Ad. Drug Delivery Rev.*, 47:1, 2001.

[44] M. Kersten. Dust-cored coils. *Elektrotechnische Zeitschrift*, page 1335, December 1937.

[45] Jin Au Kong. *Electromagnetic Wave Theory.* EMW Publishing, Cambridge,MA, 1998.

[46] L.D Landau and E.M. Lifshitz. *Electrodynamics of Continuous Media.* Pergamon, London,U.K., 1960.

[47] Jeffrey H. Lang and Anant Agarwal. *Foundations of Analog and Digital Electronic Circuits.* Department of Electrical Engineering and Computer Science, Massachusetts Institute of Technology, Cambridge,MA, 1998.

[48] Given F.J. Legg, V.E. Compressed powdered molybdenum permalloy for inductors. *Bell System Technical Journal*, page 385, July 1940.

[49] Amanda; Halas Naomi; West Jennifer; Drezek Rebekah. Loo, Christopher; Lowery. *Nano Letters*, 5(4):709–711, 2005.

[50] Caldwell W.B. Peng X. Alivisatos A.P. Loweth, C.J. and P.G. Schultz. Dna-based assembly of gold nanocrystals. *Angew.Chem., Int.Ed. Engl.*, 38:1808–1812, 1999.

[51] R. Ludwig and P. Bretchko. *RF Circuit Design Theory and Applications.* Prentice-Hall Publications, 2000.

[52] Brezovich I A; Lilly M B; Meredith R F; Weppelmann B; Henderson R A; Brawner W Jr; Salter M M. *nternational journal of hyperthermia : official journal of European Society for Hyperthermic Oncology, North American Hyperthermia Group*, 6(1):117–30, Jan-Feb 1990.

[53] M. et al. Ma. Size dependence of specific power absorption of fe3o4 particles in ac magnetic field. *Journal of Magnetism and Magnetic Materials*, 268(1-2):33–39, 2004.

[54] Shorey W. Gilchrist R.K. Barker W. Medal, B.S. and R. Hanselman. Controlled radio-frequency generator for production of localized heat in intact animal. *A.M.A. Archives of Surgery*, 79:427–431, 1959.

[55] Medhurst. *Wireless Engineer*, page 35, March 1947.

[56] X. Michalet, F. F. Pinaud, L. A. Bentolila, J. M. Tsay, S. Doose, J. J. Li, G. Sundaresan, A. M. Wu, S. S. Gambhir, and S. Weiss. Quantum dots for live cells, in vivo imaging, and diagnostics. *Science*, pages 538–544, 28 January, 2005.

[57] L. Neel. Influence of thermal fluctuations on the magnetization of ferromagnetic small particles. *C.R.Acad.Sci.*, 228:664–668, 1949.

[58] C.M. Niemeyer. Nanoparticles,proteins, and nucleic acids: Biotechnology meets materials science. *Angew.Chem., Int.Ed. Engl.*, 40:4128–4158, 2001.

[59] T.H. Oddie. Magnetic measurements on iron powders. *Journal of Scientific Instuments*, page 154, Sept. 1944.

[60] M. O'Hara. *Modeling Non-Ideal Inductors in SPICE.* Newport Components, U.K., Nov 1993.

[61] Leon R.; Halas Naomi J.; Payne J. D.; West Jennifer L. O'Neal, D. P.; Hirsch. *Proceedings of SPIE-The International Society for Optical Engineering*, 5689:149–157, 2005.

[62] C.D. Owens. Analysis of losses in magnetic cores. *Bell Laboratory Record*, page 117, Dec. 1940.

[63] J. Nadobny R. Felix in: M.H. Seegenschmiedt P. Fessenden C.C. Vernon (Eds.) P. Wust, M. Seebass. *Thermoradiotherapy and Thermochemotherapy, Vol. 1, Biology, Physiology, and Physics.* Springer, Berlin, 1996.

[64] Connolly J. Jones S.K Pankhurst, Q.A. and J. Dobson. Applications of nanoparticles in biomedicine. *J.Phys. D: Appl. Phys.*, 36:R167–R181, 2003.

[65] in: M.H. Seegenschmiedt P. Fessenden C.C. Vernon (Eds.) P.K. Sneed, B. Stea. *Thermoradiotherapy and Thermochemotherapy, Vol. 2.* Springer, Berlin, 1996.

[66] F.E. Planer. Measurement of 'q'. *Electronic Engineering*, page 453, April 1941.

[67] Rosensweig R.E. Popplewell J. and Johnston R.J. Magnetic field induced rotations in ferrofluids. *IEEE Trans. Magn.*, 26:1852–1854, 1990.

[68] Jordan A; Scholz R; Wust P; Fahling H; Krause J; Wlodarczyk W; Sander B; Vogl T; Felix R. *International journal of hyperthermia : official journal of European Society for Hyperthermic Oncology, North American Hyperthermia Group*, 13(6):587–605, Nov-Dec 1997.

[69] Stahl H; Wust P; Maier-Hauff K; Seebass M; Mischel M; Gremmler M; Golde G; Loffel J; Felix R. *Strahlentherapie und Onkologie : Organ der Deutschen Rontgengesellschaft ... [et al]*, 171(9):510–24, Sep 1995.

[70] V.V.L. Rao. The q-meter. *Proceedings of the American Institution of Radio Engineers*, page 502, Nov. 1942.

[71] M. Reed. Eddy-currents in laminated cores. *Journal of the Institution of Electrical Engineers*, page 485, May 1937.

[72] R. E. Rosensweig. Heating magnetic fluid with alternating magnetic field. *Journal of Magnetism and Magnetic Materials*, 252:370–374, 2002.

[73] C. R. Vessely L. G. Catterall S. R. Rudge, T. L. Kurtz and D. L. Williamson. *Biomaterials*, 21:1411, 2000.

[74] M. Shliomis. Magnetic fluids. *Sov. Phys. Uspekhi (Engl. Transl.)*, 17(2):153, 1974.

[75] A. Bogdnaov K. Poss T. J. Brady T. T. Shen, A. Bogdanov and R. Weisleder. *Bioconjugate Chem.*, 7:311, 1996.

[76] Marc Thompson. Simple models and measurments of magnetically induced heating effects in ferromagnetic fluids. *IEEE Transactions on Magnetics*, 34(5):3755–3764, September, 1998.

[77] Jianwu; McDonald Michael A.; Bernardo Marcelino; Hunter Finie; Zhang Yantian; Li King; Bednarski Mark; Guccione Samira. Vuu, Kien; Xie. *Bioconjugate Chemistry*, 16(4):995–999, 2005.

[78] V.G. Welsby. *The Theory and Design of Inductance Coils.* MACDONALD and Co. Ltd., London, 1950.

[79] V.G. Welsby. Dust-cored coils. *Electronic Engineering*, page 96, August 1943.

[80] V.G. Welsby. Measurement of loss coefficients of dust cores. *Post Office Electrical Engineers' Journal*, page 46, July 1942.

[81] S. et al. Xiao. Selfassembly of metallic nanoparticle arrays by dna scaffolding. *Journal of Nanoparticle Research*, 4:313–317, 2002.

[82] Markus Zahn. *Electromagnetic Field Theory: A Problem Solving Approach.* Krieger Publishing Company, Malabar,Florida 32950, 2003.

[83] Yushkanov A.A. Zavitaev, E.V. and Y.I. Yalamov. Absorption of electromagnetic radiation by a cylindrical metal particle. *Tech. Phys.*, 46:1460–1464, 2001.